

## The Roles of Tidal Marshes in the Estuarine Biochemical Processes: A Numerical Modeling Study

Xun Cai<sup>1,2</sup> , Jian Shen<sup>1</sup> , Yinglong J. Zhang<sup>1</sup> , Qubin Qin<sup>1</sup> , and Lewis Linker<sup>3</sup>

<sup>1</sup>Virginia Institute of Marine Science, William & Mary, Gloucester Point, VA, USA, <sup>2</sup>ORISE Research Participation Program at EPA, Chesapeake Bay Program Office, Annapolis, MD, USA, <sup>3</sup>U.S. Environmental Protection Agency Chesapeake Bay Program Office, Annapolis, MD, USA

### Key Points:

- A new dynamic marsh model coupled with 3D estuary model is developed to study impacts of tidal marshes on estuarine biochemical processes
- Model suggests tidal marshes drive the diurnal dissolved oxygen cycle, which increases denitrification and can enhance bottom phosphate release
- This study advances the eutrophication modeling and enhances the understanding of the tidal marsh biogeochemistry affecting the estuary

### Correspondence to:

X. Cai,  
ncai@vims.edu;  
xcai@chesapeakebay.net

### Citation:

Cai, X., Shen, J., Zhang, Y. J., Qin, Q., & Linker, L. (2023). The roles of tidal marshes in the estuarine biochemical processes: A numerical modeling study. *Journal of Geophysical Research: Biogeosciences*, 128, e2022JG007066. <https://doi.org/10.1029/2022JG007066>

Received 27 JUN 2022  
Accepted 23 JAN 2023

### Author Contributions:

**Conceptualization:** Xun Cai, Jian Shen, Qubin Qin, Lewis Linker  
**Data curation:** Xun Cai, Qubin Qin  
**Formal analysis:** Xun Cai  
**Funding acquisition:** Lewis Linker  
**Investigation:** Xun Cai, Jian Shen, Qubin Qin  
**Methodology:** Xun Cai, Jian Shen, Yinglong J. Zhang, Lewis Linker  
**Project Administration:** Lewis Linker  
**Resources:** Yinglong J. Zhang  
**Software:** Xun Cai, Yinglong J. Zhang  
**Supervision:** Jian Shen, Yinglong J. Zhang  
**Validation:** Xun Cai, Jian Shen  
**Visualization:** Xun Cai  
**Writing – original draft:** Xun Cai  
**Writing – review & editing:** Jian Shen, Yinglong J. Zhang, Qubin Qin

© 2023. The Authors.

This is an open access article under the terms of the [Creative Commons Attribution License](https://creativecommons.org/licenses/by/4.0/), which permits use, distribution and reproduction in any medium, provided the original work is properly cited.

**Abstract** Observations suggest that the existence of tidal marsh can alter the oxygen and nutrient dynamics in adjacent water bodies, but assessing the impacts of large tidal marshes on an estuary is challenging. In this study, we use a modeling approach to investigate the roles of tidal marshes on the estuarine biochemical processes. The marsh model, which simulates the ecological functions of marshes at seasonal and annual time-scales, is embedded inside an unstructured-grid three-dimensional hydrodynamic and eutrophication model (SCHISM-ICM). This modeling system simulates the growth and metabolism of the tidal marshes and links biological processes to nutrient dynamics in the water column and sediment. This model dynamically simulates nutrient recycling and physical transport of the materials between marshes and open water through wetting-drying processes. This coupled model system is validated and successfully applied to the York River Estuary. Model results suggest that tidal marshes influence the local diurnal dissolved oxygen (DO) cycle by exporting dissolved organic carbon and high sediment oxygen demand in the marsh system through the tidal exchange. The high deposition rates of organics and diurnal DO cycle enhance the sediment release of phosphorus. On the other hand, marshes tend to decrease dissolved inorganic nitrogen in the water column by settling particulate nutrients and enhancing the denitrification process. The study demonstrates that tidal marshes exert substantial impacts on the estuarine biochemical processes. The developed tidal marsh model enhances eutrophication modeling and advances the understanding of the feedback effects between marsh biogeochemistry and estuarine eutrophication processes on a systemic scale.

**Plain Language Summary** Tidal marshes are significant components in the estuarine ecosystem and are known to modify the estuarine biochemical processes. To complement the spatial and temporal limitations of field observation and experiments, we developed a modeling tool to study the role of tidal marshes. This model simulates the marsh biomass dynamics on seasonal and annual time scales. This marsh model is embedded in a complex 3D hydrodynamic-water quality model (SCHISM-ICM), so it explicitly includes the interactions of tidal marshes and the nutrient dynamics in the water column and sediment. We successfully implemented this coupled model in the York River Estuary, where extensive tidal marshes exist. This modeling study demonstrates that tidal marshes drive the local diurnal dissolved oxygen (DO) cycles and low-DO events. In addition, tidal marshes tend to increase the phosphate release from the sediment but decrease the dissolved inorganic nitrogen in the water column. Overall, tidal marshes have substantial impacts on the estuarine biochemical processes.

## 1. Introduction

Highly productive tidal marshes play a key role in the estuarine ecosystem by affecting the dynamics of carbon, nitrogen, phosphorus, and oxygen (Bridgman et al., 2006; Chmura et al., 2003). Sedimentation is greatly enhanced in the tidal marshes due to enhanced flow impedance locally and the tidal marshes tend to be traps of particulate material, therefore retaining a significant amount of carbon and other nutrients (Bowden et al., 1991; Grant & Patrick, 1970; Sundareshwar et al., 2003; Ziegler et al., 1999); in addition, dissolved nutrients are also observed to be exported or filtered from the tidal marshes in some systems (Anderson et al., 1997; Axelrad et al., 1976; Chambers et al., 1992; Jordan et al., 1983). In some areas, the tidal marshes tend to export excess materials, including organic carbon and other nutrients, into adjacent waters and thus enhance estuarine productivity in these systems (Alongi, 2020; Chicharo et al., 2008; Czaplá et al., 2020; Odum et al., 1984; Ridd et al., 1988; Tzortziou et al., 2011). Differing results of the exported or filtered dissolved organic carbon are observed at different estuaries (Bukaveckas, 2021; Czaplá et al., 2020; Neubauer & Anderson, 2003). The remineralization of the

abundant organic matter, which can be directly exported from the marshes or from the increased local estuarine productivity, is suggested to cause excessive consumption of dissolved oxygen (DO) (Diaz & Rosenberg, 2001; Levin et al., 2009). The observed low-DO events (hypoxia when DO concentration is lower than  $2 \text{ mg L}^{-1}$ ) near tidal marshes usually follow a diurnal pattern, with lower DO occurring at low tide (Swarth & Peters, 1993). Also, bottom fluxes of ammonium and phosphate can be enhanced due to the marsh-induced low-DO events or the low sediment redox potentials (Lai & Lam, 2008). Therefore, tidal marshes play an important role in modifying the estuarine biochemistry on variable time scales and in different systems. The complex dynamics and interaction of marsh and estuarine water are difficult to fully observe or analyze. Studies using observational methods to investigate the role of tidal marshes usually focus on a limited number of small systems due to the difficulty in conducting the measurements and calculations. On the other hand, numerical models can investigate individual processes in isolation by doing immeasurable scenarios. In addition, modeling studies can be applied at a larger spatial scale (e.g., the York River Estuary in this paper) to study the role of tidal marshes on estuarine biochemical processes.

Current marsh models usually focus on the long-term processes of marsh morphology and evolution on decadal to centennial timescales (Alizad et al., 2016; Fagherazzi et al., 2004; Kirwan & Murray, 2007; Marani et al., 2007; Morris et al., 2002; Townend et al., 2011). These models usually account for the feedback between marsh biomass, platform elevation, and sedimentation, with no particular attention paid to biochemical processes in the estuarine water outside the marshes (Alizad et al., 2016; Fagherazzi et al., 2012; Morris et al., 2002). On the other hand, another type of marsh model mainly focuses on the biological functions of the marsh plants and their impacts on the surrounding system on seasonal to annual timescales (Buzzelli et al., 1999; Cerco & Tian, 2021). However, this type of marsh model is mostly used as an offline box model using additional source/sink terms to represent marsh function in the water quality variables' mass balance equation, in which marsh growth, respiration, and nutrient cycles are not coupled into hydrodynamic-water quality models for system-wide simulations due to the challenges of fine resolution as required to account for the marsh irregularities, such as the varying patches of tidal marsh wetlands. Also, the tidal marshes are usually not physically included in the grid domain in these models for the complex wetting and drying processes in these regions. Ideally, the marsh habitat studies would require the model domain coverage to include the intertidal flooding zone as well as the surrounding environment, so the numerical model must be sufficiently robust to handle the inundation processes (Zhang et al., 2020).

In this study, we developed a new marsh modeling approach for studying the role of the tidal marsh on estuarine biochemical processes. This marsh model is integrated into an unstructured-grid three-dimensional hydrodynamics and water quality model to simulate both physical and biogeochemical processes in an entire estuarine system, including the marsh wetlands and the surrounding waters. The marsh-induced form drag is included in the momentum equation, and the marsh-induced turbulence is added as an additional source term in the turbulence closure equations (Zhang et al., 2020). This model explicitly simulates the interactions between marsh and estuarine biochemical processes, such as the nutrient release from the marsh metabolism and bottom sediment to the water column. By fully coupling hydrodynamic, water quality, and marsh modules, we can simultaneously simulate the multiple nonlinear interactions between the physiological processes of the marsh, physical processes, and biochemical processes in an estuary (the York River Estuary). This process-based model can be used to study the effects of tidal marshes on water quality on a relatively large regional scale (e.g., the York River Estuary and the Chesapeake Bay), to complement direct observations. The seasonal to annual temporal scale is targeted by this model, and the morphological changes are not considered here.

In the Methods section, we describe the study site, available data, model development, a benchmark for its development, model implementations, the design of sensitivity tests, and the analysis methods. In the Results section, we present the model skill assessments for its implementation in the York River Estuary, which include the simulation of the physical environment, the major water quality properties, and marsh biomass and productivity. In the Discussion section, we discuss the roles of the tidal freshwater marshes on the biochemical processes by focusing on the responses of estuarine nutrients and phytoplankton as revealed by the sensitivity tests, especially a marsh removal scenario (NVO) that omits the ecological functions of the marsh. We will also discuss the uncertainty and limitations of the current model framework and the direction of future studies. Conclusions are summarized in the final section.

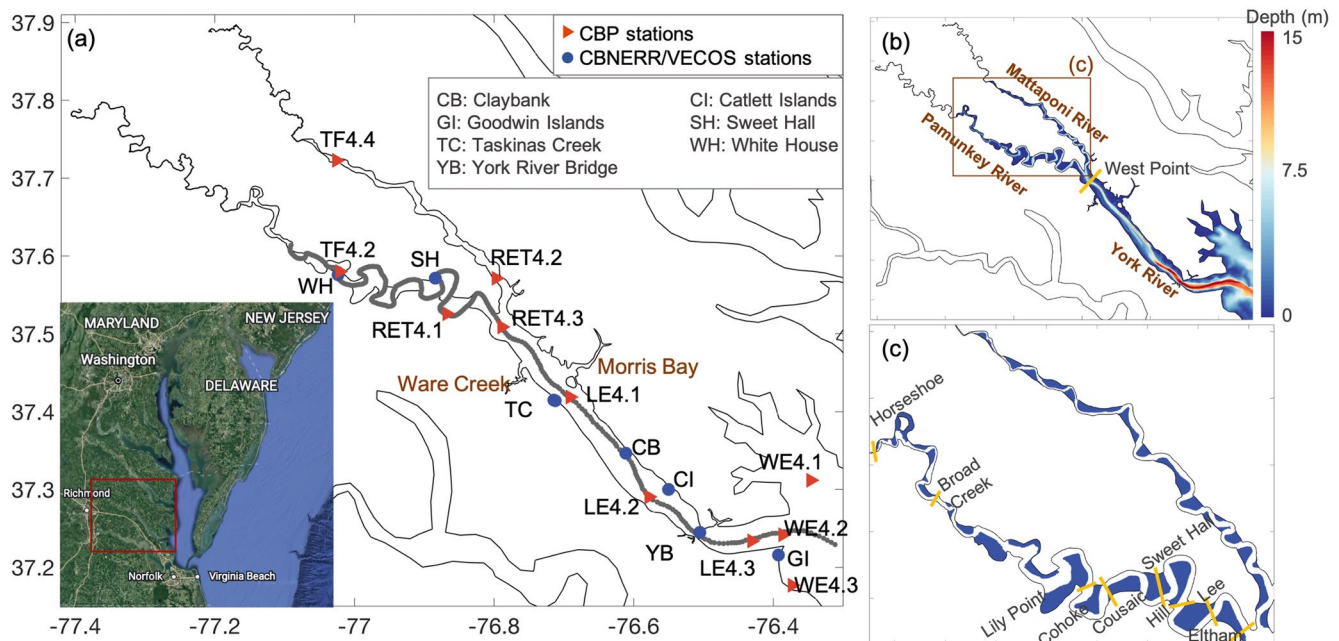


**Figure 1.** (a) The York River Estuary. The red triangles denote the Chesapeake Bay Program (CBP) stations, and the blue circles denote the stations from Chesapeake Bay National Estuarine Research Reserve (CBNERR) and Virginia Estuarine and Coastal Observing System (VECOS). The gray line denotes the along-channel transect used in this study. (b) Bathymetry of the study area. (c). Extensive and fringing marshes in the Pamunkey-Mattaponi River System. The blue polygons denote the marshes along the Pamunkey River and the Mattaponi River based on the USGS topography map. Yellow lines in panels (b, c) denote the interface to calculate the material exchange in this study.

## 2. Methods

### 2.1. Study Site and Available Data

The Pamunkey River and Mattaponi River are tidal rivers joined at West Point, Virginia (VA) to form the York River (Figure 1), which is one of the major tributaries in the lower Chesapeake Bay (the Bay thereafter). The mean discharge of the Pamunkey River and Mattaponi Rivers are  $28.7$  and  $14.4 \text{ m}^3 \text{ s}^{-1}$ , respectively, but the total discharge into the York from these two rivers can be more than  $107 \text{ m}^3 \text{ s}^{-1}$  during wet seasons (Shen & Haas, 2004). The York estuary is a micro-tidal estuary, whose mean tidal range increases from  $0.7 \text{ m}$  at the mouth to  $0.85 \text{ m}$  at the West Point and exceeds  $1.0 \text{ m}$  at the heads of the Pamunkey and Mattaponi Rivers according to the historical data ([https://tidesandcurrents.noaa.gov/historic\\_tide\\_tables.html](https://tidesandcurrents.noaa.gov/historic_tide_tables.html)). The Pamunkey-Mattaponi-York system has a mean residence time of 104 days under the mean flow condition (Shen & Haas, 2004). The upper portion of the Pamunkey and Mattaponi Rivers are tidal fresh while the location of the transition from brackish to freshwater varies with river discharge (Shen & Haas, 2004). Salinity at West Point ranges from 0 to 20 PSU and varies with freshwater discharge (<https://www.chesapeakebay.net/what/data>). The annual temperature follows a seasonal trend with  $25.7^\circ\text{C}$  at annual highs and  $0.9^\circ\text{C}$  at annual lows (Brooks, 1983). The average precipitation is about  $95.9 \text{ cm}$  in this region, typically the highest in July and August (Brooks, 1983). Waves are usually considered to be insignificant in this region (Friedrichs, 2009).

The Pamunkey River has over  $28.9 \text{ km}^2$  of tidal marshes and forested wetlands adjacent to the meandering channels, located within  $72 \text{ km}$  of West Point (Figure 1; Perry, 1991; Mitchell et al., 2017). On the Mattaponi side, tidal marshes are found from West Point to approximately  $50 \text{ km}$  upstream, occupying an area of  $21.7 \text{ km}^2$  (Figure 1; Mitchell et al., 2017). These marshes, as marked in Figure 1c, account for 97.27% of the total marsh coverage in the York River Estuary, excluding the extensive or embayed marshes in the sheltered sub-tributaries such as Morris Bay and Ware Creeks (Figure 1a; Mitchell et al., 2017). Overall, there is a continuum of marsh types from tidal oligohaline marshes to non-tidal freshwater marshes along the Pamunkey and Mattaponi Rivers (Perry, 1991). The total area of tidal freshwater and brackish marshes along the Pamunkey and Mattaponi Rivers has changed little ( $<0.009\%$ ) over the past 40 years, although the brackish marshes have replaced some tidal freshwater species (Mitchell et al., 2017).

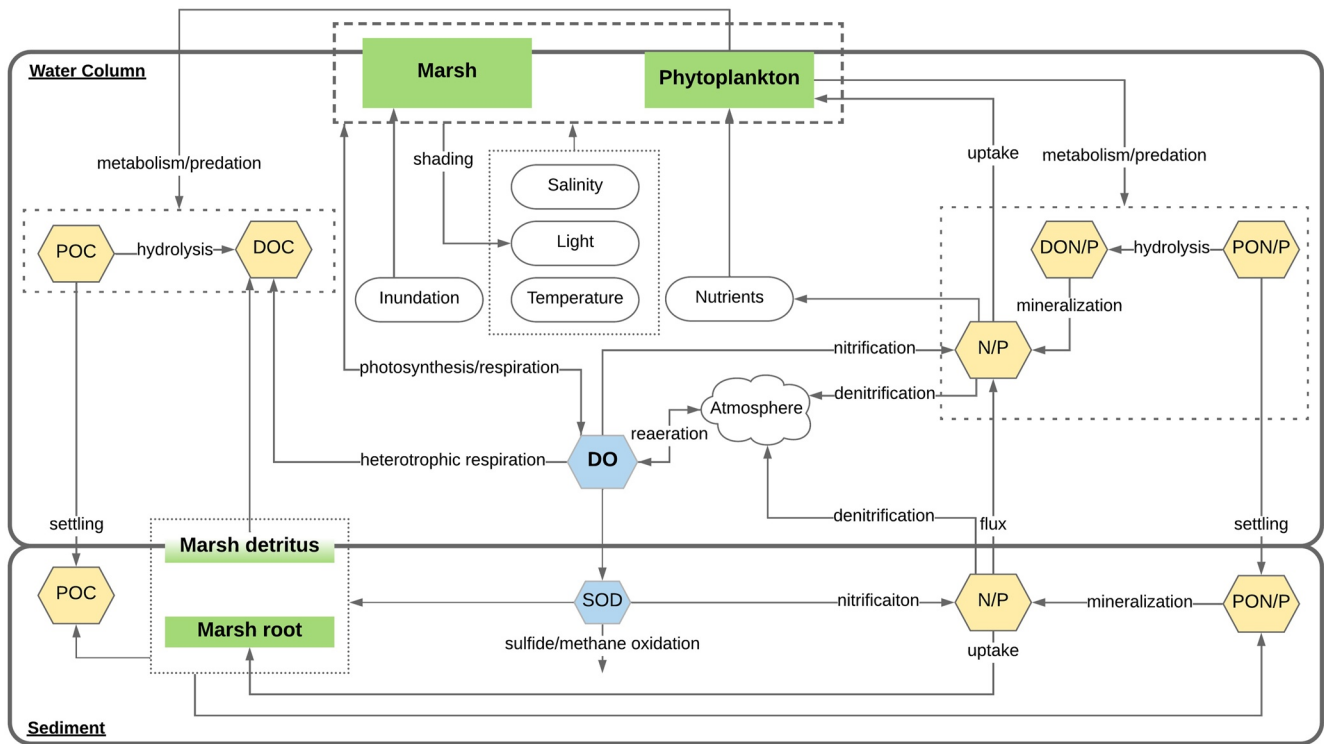


Figure 2. Coupled ICM-Marsh model diagram.

We utilize the database of water quality monitoring networks in the York River Estuary from the Chesapeake Bay Program (CBP; <https://www.chesapeakebay.net/what/data>), which has a wide coverage of variables—including nutrients, sediments, planktons, water temperature, salinity, and DO. The frequency of these measurements is once (winter) or twice (summer) each month. This database has full spatial coverage from the tidal freshwater region to the mouth of the York River (Figure 1). In addition to this database, we also use some high-frequency (15-min interval) observations of salinity and elevation from the Chesapeake Bay National Estuarine Research Reserve (CBNERR; <http://cdmo.baruch.sc.edu>) and Virginia Estuarine and Coastal Observing System (VECOS; <http://vecos.vims.edu>). The delineation of the marshes follows the USGS topography map ([https://www.usgs.gov/core-science-systems/national-geospatial-program/us-topo-maps-america?qt-science\\_support\\_page\\_related\\_con=0#qt-science\\_support\\_page\\_related\\_con](https://www.usgs.gov/core-science-systems/national-geospatial-program/us-topo-maps-america?qt-science_support_page_related_con=0#qt-science_support_page_related_con)).

## 2.2. Model Development

### 2.2.1. Model Framework

The fully coupled hydrodynamic-water quality-marsh model was developed within the Semi-implicit Cross-scale Hydroscience Integrated System Model (SCHISM), an open-source community-supported modeling system (Zhang et al., 2016). SCHISM provides physical transport fields to the water quality Integrated Compartment Model (ICM; Cerco & Cole, 1994) in this framework. ICM was developed by the U.S. Army Corps of Engineer Research and Development Center, and was fully integrated inside SCHISM (Cai et al., 2020). Besides the 21 water quality variables (e.g., phytoplankton, carbon, nitrogen, phosphorus, and oxygen), benthic algae are also included in this model (Cerco & Seitzinger, 1997). This modeling system also includes the sediment flux model developed by Di Toro and Fitzpatrick (1993), which simulates the deposition and diagenesis processes of particulate organic matter, the recycling of inorganic nutrients to the water column, and the sediment oxygen demands. In this coupled water quality model, the interactions between phytoplankton, oxygen, and nutrients in both the water column and sediment are simulated (Figure 2). The growth of phytoplankton is controlled by temperature, light availability, nutrient supplies, and salinity, which is specifically a controlling factor for diatoms. The growth of phytoplankton produces oxygen and consumes inorganic nutrients (nitrogen and phosphorus), while the respiration and predation of phytoplankton consume oxygen and release nutrients in multiple forms (e.g., inorganic

nutrients, dissolved organic nutrients, and labile and refractory particulate organic nutrients). Oxygen is also consumed by heterotrophic respirations, nitrifications, and other oxidation processes in the sediment, while the atmosphere can be a source of surface water oxygen. Particulate organic nutrients (carbon, nitrogen, and phosphorus) hydrolyze to dissolve organic nutrients, and dissolved organic nutrients are mineralized into inorganic nutrients. Specifically for nitrogen, the nitrification process transforms ammonium to nitrate, and the denitrification process removes the nitrate from the system and releases it to the atmosphere as nitrous oxide and nitrogen gas. Both the nitrification and denitrification processes are controlled by the local oxygen concentration. High oxygen tends to prompt nitrification while low oxygen is favorable to the denitrification process. The nitrification and denitrification are expressed as follows (Cercio & Cole, 1994):

$$\text{Nit} = \frac{\text{DO}}{\text{KHont} + \text{DO}} \cdot \frac{\text{NH}_4}{\text{KHnt} + \text{NH}_4} \cdot f(T) \cdot \text{NTm} \quad (1)$$

$$\text{Denit} = \text{ANDC} \cdot \frac{\text{KHor}}{\text{KHor} + \text{DO}} \cdot \frac{\text{NO}_3}{\text{KHdn} + \text{NO}_3} \cdot \text{AANOX} \cdot \text{KDOC} \cdot \text{DOC} \quad (2)$$

where Nit ( $\text{g N m}^{-3} \text{ d}^{-1}$ ) is nitrification rate and Denit ( $\text{g N m}^{-3} \text{ d}^{-1}$ ) is denitrification rate. DO, NH<sub>4</sub>, NO<sub>3</sub>, and DOC refers to the concentrations of dissolved oxygen ( $\text{g O}_2 \text{ m}^{-3}$ ), ammonium ( $\text{g N m}^{-3}$ ), nitrate ( $\text{g N m}^{-3}$ ), and dissolved organic carbon ( $\text{g C m}^{-3}$ ) respectively. KHont ( $\text{g O}_2 \text{ m}^{-3}$ ) and KHnt ( $\text{g N m}^{-3}$ ) are half-saturation constants of DO and NH<sub>4</sub> for nitrification respectively.  $f(T)$  is a temperature adjustment for nitrification where nitrification is the maximum NTm ( $\text{g N m}^{-3} \text{ d}^{-1}$ ) when the temperature is optimal. ANDC ( $\text{g N per g C}$ ) refers to the mass of nitrate nitrogen reduced per mass of dissolved organic carbon oxidized. KHor ( $\text{g O}_2 \text{ m}^{-3}$ ) and KHdn ( $\text{g N m}^{-3}$ ) are half-saturation constants of DO for oxic respiration and NO<sub>3</sub> for denitrification respectively. KDOC ( $\text{d}^{-1}$ ) is heterotrophic respiration rate of DOC when oxygen is infinitely sufficient, and KDOC is also affected by temperature. AANOX is the ratio of denitrification rate to oxic dissolved organic carbon respiration rate. So that significant decomposition of DOC by denitrification occurs only when nitrate is sufficient and oxic respiration is limited by the availability of DO. In terms of phosphorus, the bottom flux of the recycled inorganic phosphate largely increases under low-DO events (DO concentration  $<1.0 \text{ g m}^{-3}$ ) due to high desorption under anaerobic condition (Di Toro & Fitzpatrick, 1993).

We developed the marsh module using a similar approach to the submerged aquatic vegetations (SAV) module (Cai, 2018), but we modified and added specific processes of marsh plants. On the physical side, the marsh-induced drag force and 3D turbulence were fully incorporated into the hydrodynamic model, and the interaction between the marsh and hydrodynamics was dynamically simulated (Zhang et al., 2020). Biologically, three types of marshes (salt marsh, brackish marsh, and freshwater marsh) were added to the group of primary producers in the ecosystem model. The primary producers (e.g., phytoplankton and marsh plants) interact with each other through competition for light and nutrient supplies (Figure 2). Details of this tidal marsh model are described in the next two sub-sections.

### 2.2.2. Tidal Marsh Model

The kinetic marsh model shares a similar structure as the submerged aquatic vegetation model (Cai, 2018; Cercio & Moore, 2001). The marsh plant is divided into three tissues that are modeled, respectively—leaf, stem, and root. The leaf is the only tissue that is photosynthetic and transfers its production to other tissues. The growth of the leaf is controlled by multiple limiting factors—temperature, light supplies, salinity stress, and inundation pressure. Although nutrients can affect plant growth, the nutrient supply from the sediment is assumed to be sufficient to support the growth of the marsh, and marsh roots can reach deep or far areas to adjust to the nutrient supply. Thus, the nutrients are not considered as a limiting factor in this model. Inundation stress is suggested by the observations to be included in the model design because a longer inundation duration and deeper flooding tend to reduce marsh growth (Janousek & Mayo, 2013; McHugh & Dighton, 2004; Watson et al., 2015). The above-ground biomass is reduced by leaf and stem metabolism, primarily defoliation. The plant height is calculated as a linear function of the above-ground biomass. The mathematical formulas for the biomass of the three tissues and the canopy height are:

$$\frac{d\text{LF}}{dt} = \text{Plf}(T, I, S, F) \cdot (1 - \text{Fam}) \cdot \text{FPlf} \cdot \text{LF} - \text{MTlf}(T) \cdot \text{BMlf}(T) \cdot \text{LF} \quad (3)$$

$$\frac{d\text{ST}}{dt} = \text{Plf}(T, I, S, F) \cdot (1 - \text{Fam}) \cdot \text{FPst} \cdot \text{LF} - \text{MTst}(T) \cdot \text{BMst}(T) \cdot \text{ST} \quad (4)$$

$$\frac{d\mathbf{RT}}{dt} = \text{Plf}(T, I, S, F) \cdot (1 - \text{Fam}) \cdot \text{FPrt} \cdot \text{LF} - \text{BMrt}(T) \cdot \mathbf{RT} \quad (5)$$

$$\mathbf{H} = \begin{cases} d \cdot (\text{LF} + \text{ST}) + e, & \text{when } (\text{LF} + \text{ST}) \leq \text{crit} \\ a \cdot (\text{LF} + \text{ST} - \text{crit}) + d \cdot \text{crit} + e, & \text{when } (\text{LF} + \text{ST}) > \text{crit} \end{cases} \quad (6)$$

where **LF**, **ST**, and **RT** ( $\text{g C m}^{-2}$ ) are biomasses of leaf, stem, and root of the marsh, respectively.  $\text{Plf}$  ( $\text{day}^{-1}$ ) is the growth function of the leaf. This growth function is determined by temperature ( $T$ ), light ( $I$ ), salinity ( $S$ ), and inundation stress ( $F$ ).  $\text{Fam}$  is the fraction for active metabolism during photosynthesis.  $\text{FPlf}$ ,  $\text{FPst}$ , and  $\text{FPrt}$  are fractions of biomass transformations from leaf photosynthesis.  $\text{BMlf}$ ,  $\text{BMst}$ , and  $\text{BMrt}$  ( $\text{day}^{-1}$ ) are basal metabolism rates of the leaf, stem, and root, respectively, which are functions of temperature.  $\text{MTlf}$  and  $\text{MTst}$  are seasonal mortalities of leaf and stem.  $\mathbf{H}$  ( $m$ ) is marsh canopy height, calculated from the above-ground biomass with the coefficients of  $\text{crit}$ ,  $a$ ,  $d$ , and  $e$ .

The growth rate of leaf  $\text{Plf}$  can be written as a product of temperature-driven maximum growth rate and three stress functions (salinity, light, and inundation):

$$\text{Plf} = \text{Pm}(T) \cdot f(S) \cdot f(I) \cdot f(F) / \text{acdw} \quad (7)$$

where  $\text{Pm}$  ( $\text{g C g}^{-1} \text{DW day}^{-1}$ ) is the maximum growth rate, which is determined by the temperature.  $f(S)$ ,  $f(I)$ , and  $f(F)$  are the limitation functions of salinity, light, and inundation stress, respectively.  $\text{acdw}$  ( $\text{g C g}^{-1} \text{DW}$ ) is the plant carbon to dry-weight ratio.

The maximum growth rate  $\text{Pm}$  is expressed as:

$$\text{Pm}(T) = \text{pmbs} \cdot e^{-\text{KTg1} \cdot (T - \text{Topt})^2}, \text{ when } T \leq \text{Topt} \quad (8)$$

$$\text{Pm}(T) = \text{pmbs} \cdot e^{-\text{KTg2} \cdot (T - \text{Topt})^2}, \text{ when } T > \text{Topt} \quad (9)$$

where  $\text{pmbs}$  ( $\text{g C g}^{-1} \text{DW day}^{-1}$ ) is the coefficient for the maximum growth rate function.  $\text{KTg1}$  and  $\text{KTg2}$  ( $^{\circ}\text{C}^{-2}$ ) are the shape coefficients of temperature adjustment.  $T$  ( $^{\circ}\text{C}$ ) is the local temperature and  $\text{Topt}$  ( $^{\circ}\text{C}$ ) is the optimal temperature for plant growth.

The limiting function of salinity  $f(S)$  is expressed as:

$$f(S) = \frac{\text{ST}}{\text{ST} + (\text{Salt} - \text{Saltopt})^2} \quad (10)$$

where  $\text{ST}$  is salinity stress coefficient ( $\text{PSU}^2$ ),  $\text{Salt}$  is water column salinity, and  $\text{Saltopt}$  ( $\text{PSU}$ ) is the optimal salinity for this species. The salinity control  $f(S)$  and flooding factor  $f(F)$  are developed as sigma curves for the growth of the marsh based on the knowledge from observations (Janousek & Mayo, 2013; Pearcy & Ustin, 1984). The limitation function of inundation stress  $f(F)$  is:

$$f(F) = \frac{\text{rdephcan}}{\text{tinun} + \text{rdephcan}} \quad (11)$$

$$\text{rdephcan} = \frac{\mathbf{H}}{\text{tdep}} \quad (12)$$

where  $\text{rdephcan}$  is the ratio of canopy height  $\mathbf{H}$  to the total water column depth  $\text{tdep}$ . The user input  $\text{tinun}$  is the inundation pressure coefficient. Once the ratio of canopy height to the total water column depth reaches  $\text{tinun}$ , the inundation limitation is 0.5; and if the ratio further increases, there is less inundation stress ( $>0.5$ ). An increase in the inundation period or inundation depth can result in an increase of the stress. In this study, the adaptive capability of the plant physiology is not considered. This limiting function can be modified or removed if the plant has the adaptive capability for the environment changes. The limiting functions of light  $f(I)$  is:

$$f(I) = \frac{\text{Iwc}}{\sqrt{\text{Iwc}^2 + \text{Ik}^2}} \quad (13)$$

$$I_k = \frac{Pm(T)}{\alpha} \quad (14)$$

$$I_{wc} = \frac{I_{atcnpy}}{K_{sh} \cdot (LF + ST)} \cdot [1 - e^{-(K_{sh} \cdot (LF + ST))}] \quad (15)$$

$$I_{atcnpy} = \begin{cases} I_o \cdot e^{-K_w \cdot (t_{dep} - H)}, & \text{when } H < t_{dep} \\ I_o, & \text{when } H \geq t_{dep} \end{cases} \quad (16)$$

where  $I_{wc}$  ( $E m^{-2}$ ) is irradiance utilized by plant growth,  $I_{atcnpy}$  ( $E m^{-2}$ ) is irradiance reaching the canopy top, and  $I_o$  ( $E m^{-2}$ ) is irradiance reaching the water surface.  $I_k$  ( $E m^{-2}$ ) is an adjustment function of leaf growth.  $K_{sh}$  ( $m^2 g^{-1}$ ) is the leaf self-shading coefficient and  $K_w$  ( $m^{-1}$ ) is the light attenuation coefficient in the water.  $K_w$  is a spatially and temporally varying parameter that is accounted for all the light attenuation that is contributed by a function of particulate organic carbon (correlated to suspended to sediment) and phytoplankton (Cerro & Noel, 2017).

The metabolism rates of the three tissues are functions of temperature:

$$BM_{lf} = BM_{lfr} \cdot e^{KT_{blf} \cdot (T - Tr_{lf})} \quad (17)$$

$$BM_{st} = BM_{str} \cdot e^{KT_{bst} \cdot (T - Tr_{st})} \quad (18)$$

$$BM_{rt} = BM_{rtr} \cdot e^{KT_{brt} \cdot (T - Tr_{rt})} \quad (19)$$

where  $BM_{lf}$ ,  $BM_{st}$ , and  $BM_{rt}$  ( $day^{-1}$ ) are basal metabolism rates of leaf, stem, and root, respectively.  $BM_{lfr}$ ,  $BM_{str}$ , and  $BM_{rtr}$  ( $day^{-1}$ ) are basal metabolism rates of leaf, stem, and root, respectively, at reference temperatures  $Tr_{lf}$ ,  $Tr_{st}$ , and  $Tr_{rt}$  ( $^{\circ}C$ ).  $KT_{blf}$ ,  $KT_{bst}$ , and  $KT_{brt}$  ( $^{\circ}C^{-1}$ ) are the shape coefficients for the temperature functions of leaf, stem, and root, respectively.

A sigmoid function is used as the seasonal mortality coefficient to account for the natural decay of aboveground plants in the fall. These mortality coefficients are expressed as a function of temperature (Li et al., 2021):

$$MT_{lf} = \frac{ad_{lf}}{1 + e^{-bd_{lf} \cdot (T - cd_{lf}) - dd_{lf}}} + 1 \quad (20)$$

$$MT_{st} = \frac{ad_{st}}{1 + e^{-bd_{st} \cdot (T - cd_{st}) - dd_{st}}} + 1 \quad (21)$$

where  $MT_{lf}$  and  $MT_{st}$  are seasonal mortality coefficients of leaf and stem, respectively. The magnitude of  $MT_{lf}$  and  $MT_{st}$  are determined by the parameters  $ad_{lf}$  and  $ad_{st}$ . The seasonal variability of  $MT_{lf}$  and  $MT_{st}$  is determined by  $bd_{lf}$ ,  $cd_{lf}$ ,  $dd_{lf}$ ,  $bd_{st}$ ,  $cd_{st}$ , and  $dd_{st}$ .

### 2.2.3. Linkage Between the Tidal Marsh Model and Water Quality Model

This tidal marsh model is linked to the water quality model primarily by accounting for nutrient uptakes directly from the sediment and the releases from the decay of marsh detritus to the various groups of nutrients in the water column and sediment. The growth of leaf takes up ammonia and phosphate from the sediment directly:

$$\text{uptake}_{NH_4} = -Anc \cdot Plf \cdot LF \quad (22)$$

$$\text{uptake}_{PO_4} = -Apc \cdot Plf \cdot LF \quad (23)$$

where  $\text{uptake}_{NH_4}$  and  $\text{uptake}_{PO_4}$  ( $g m^{-2} day^{-1}$ ) are uptake of ammonia and phosphate from the sediment deeper layer to support plant growth, respectively.  $Anc$  ( $g N g^{-1} C$ ) and  $Apc$  ( $g P g^{-1} C$ ) are nitrogen and phosphorus to carbon ratios, respectively.

The metabolism of leaf and stem, mostly defoliation, settles organic matters to the bottom. In addition, the metabolism of the roots also releases particulate organic nutrients to the sediment. The PON and POP budget in the sediment is fueled by both sources that are expressed as:

$$\text{setPON} = \text{Anc} \cdot [(\text{Plf} \cdot \text{Fam} + \text{MTlf} \cdot \text{BMlf}) \cdot \mathbf{LF} + \text{MTst} \cdot \text{BMst} \cdot \mathbf{ST} + \text{BMrt} \cdot \mathbf{RT}] \quad (24)$$

$$\text{setPOP} = \text{Apc} \cdot [(\text{Plf} \cdot \text{Fam} + \text{MTlf} \cdot \text{BMlf}) \cdot \mathbf{LF} + \text{MTst} \cdot \text{BMst} \cdot \mathbf{ST} + \text{BMrt} \cdot \mathbf{RT}] \quad (25)$$

$$\frac{d\text{PON}(1 : 3)}{dt} = \text{setPON} \cdot \text{frnveg}(1 : 3) \quad (26)$$

$$\frac{d\text{POP}(1 : 3)}{dt} = \text{setPOP} \cdot \text{frpveg}(1 : 3) \quad (27)$$

where setPON and setPOP ( $\text{g m}^{-2} \text{ day}^{-1}$ ) are sources of particulate organic matter to the lower layer of the sediment, respectively. frnveg and frpveg are the fractions of these particulate nutrients going to three groups of labile, refractory, inert groups in the sediment budget of PON and POP. Both the dissolved organic nitrogen and phosphorus hydrolyzed and the inorganic nutrients mineralized from the marsh detritus in the pore water of the upper sediment layer are assumed to be relatively minor and neglected in this model. Regarding the whole system, the marsh will affect the local nitrification-denitrification process by both directly affecting the nitrogen pool (e.g., by taking up sediment ammonia and settling particulate organic nitrogen) and indirectly affecting the local oxygen and organic carbon, which eventually modify the nitrogen dynamics.

When the plant is fully submerged, the net production of oxygen by leaf photosynthesis minus the consumption from active metabolism during photosynthesis is accounted as a source to the water column oxygen, but when the plant is partially submerged or totally above the water surface, we assume the oxygen produced by the marsh goes to the atmosphere directly. Once submerged, the contribution of the marsh is added as a source term to the water column DO in the vertical cells that the marsh occupies:

$$\frac{d\text{DO}}{dt} = \text{Aocr} \cdot \text{Plf} \cdot (1 - \text{Fam}) \cdot \mathbf{LF/H} \quad (28)$$

where DO ( $\text{g m}^{-3}$ ) is oxygen concentration in the vertical layers of the water column where marsh occupies and Aocr ( $\text{g O}_2 \text{ g}^{-1} \text{ C}$ ) is oxygen to carbon ratio. On the other hand, the defoliation settles onto the sediment, part of it is assumed to be hydrolyzed in the pore water of the upper sediment layer and consumes the available oxygen diffused from the bottom layer of the water column. In addition, the metabolism of roots also consumes oxygen. Both processes contribute to the sediment oxygen demand:

$$\text{sedDO} = -\text{Aocr} \cdot \left[ \text{FrtDO} \cdot \text{BMrt} \cdot \mathbf{RT} + \text{FDO} \cdot \frac{\text{DO}_0}{\text{KHR} + \text{DO}_0} \cdot (\text{MTlf} \cdot \text{BMlf} \cdot \mathbf{LF} + \text{MTst} \cdot \text{BMst} \cdot \mathbf{ST}) \right] \quad (29)$$

where sedDO ( $\text{g m}^{-2} \text{ day}^{-1}$ ) is sediment oxygen demand driven by the marshes. FrtDO is the fraction of DO consumption in root metabolism. FDO is the fraction of the organic carbon hydrolyzed in the pore water of the upper sediment layer. KHR ( $\text{g m}^{-3}$ ) is the coefficient of DOC oxidation in the upper sediment layer. DO<sub>0</sub> ( $\text{g m}^{-3}$ ) is oxygen concentration in the bottom layer of water column. The remaining DOC in the pore water diffused into the water column:

$$\text{sedDOC} = \text{FDO} \cdot \frac{\text{KHR}}{\text{KHR} + \text{DO}_0} \cdot (\text{MTlf} \cdot \text{BMlf} \cdot \mathbf{LF} + \text{MTst} \cdot \text{BMst} \cdot \mathbf{ST}) \quad (30)$$

where sedDOC ( $\text{g m}^{-2} \text{ day}^{-1}$ ) is the DOC flux from the upper sediment layer to the water column. The rest of the organic carbon goes into the lower sediment layer as particulate matter:

$$\text{setPOC} = (1 - \text{FrtDO}) \cdot \text{BMrt} \cdot \mathbf{RT} + (1 - \text{FDO}) \cdot (\text{MTlf} \cdot \text{BMlf} \cdot \mathbf{LF} + \text{MTst} \cdot \text{BMst} \cdot \mathbf{ST}) \quad (31)$$

$$\frac{d\text{POC}(1 : 3)}{dt} = \text{setPOC} \cdot \text{frcveg}(1 : 3) \quad (32)$$

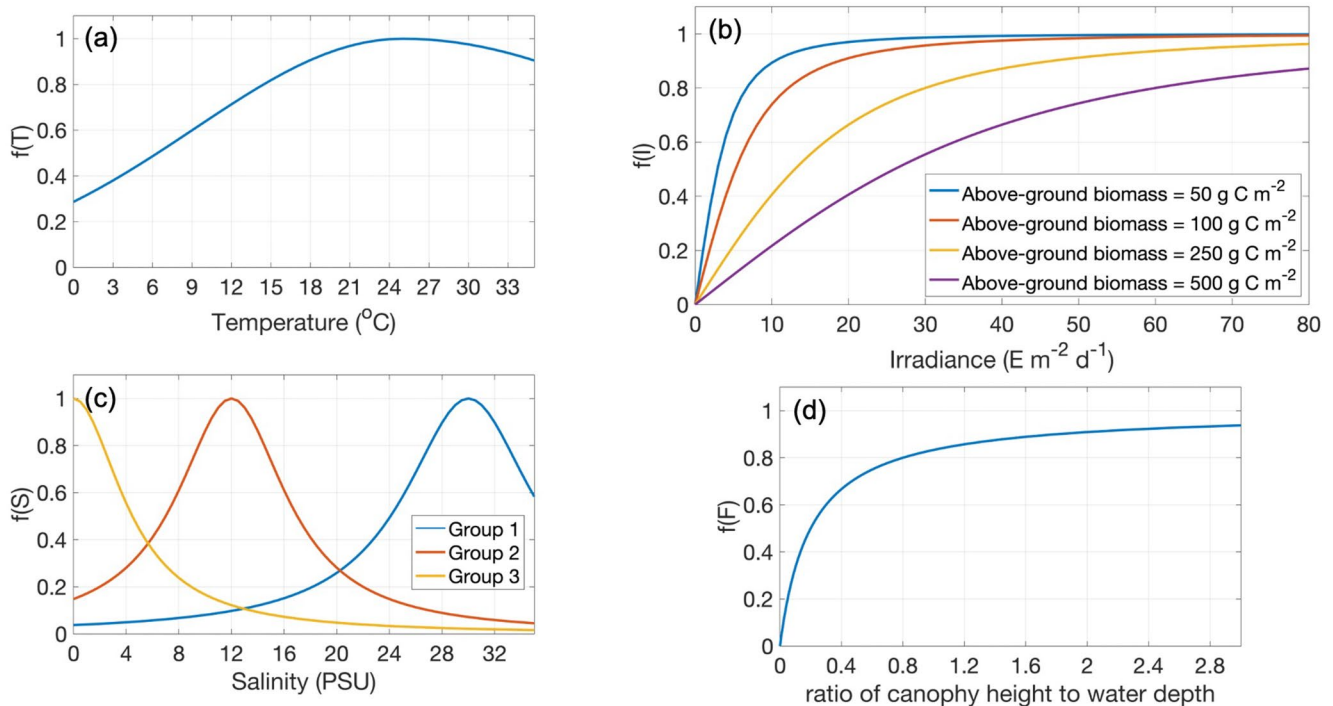


**Figure 3.** (a) Effects of temperature on marsh production, where  $f(T) = 1$  when the temperature reaches the optimal value. (b) Marsh production versus irradiance curve accounting self-shading. (c) Impacts of salinity on marsh production in the salt marsh—Group 1, brackish marsh—Group 2, and freshwater marsh—Group 3. (d) Inundation stress.

where setPOC ( $\text{g m}^{-2} \text{ day}^{-1}$ ) is a source of particulate organic carbon to the lower layer of the sediment.  $\text{frcvveg}(1 : 3)$  are the fractions of these particulate carbon going to three groups of labile, refractory, inert groups in the sediment budget of POC, respectively.

### 2.3. Model Implementation and Sensitivity Tests

The marsh dynamic process that responds to the changes in environmental conditions is demonstrated in Figure 3. Marsh reaches its maximum growth rate when the temperature reaches the optimal value for this species (Figure 3a). Higher solar radiation reaching the marsh canopy alleviates light limitation on marsh growth, while self-shading (included in the model) limits the growth if the marsh reaches high biomass (Figure 3b). The optimal salinity for the three groups of the marsh (salt marsh - Group 1, brackish marsh—Group 2, and freshwater marsh—Group 3) varies. For example, the freshwater marsh receives no salinity stress on its growth when the local salinity is close to 0 PSU, so the value of  $f(S)$  is close to 1 (Figure 3c). The plant height to water depth ratio limits marsh growth when the marsh is submerged (i.e., the ratio is less than 1); when the marsh emerges, the water depth places a minor limitation on marsh growth (Figure 3d). The parameter sets used in this study are listed in Table 1. The lack of measured parameters and data is one of the most difficult parts of developing a dynamic marsh model, which could be one of the reasons why only simple models or empirical models (Cercio & Tian, 2022) have been used to simulate marsh. We acknowledge the limitations of the model parameterization, whose values are primarily adopted or selectively modified from a published SAV model (Cai, 2018; Cercio & Moore, 2001). Without guidance from observations, the parameters are based on literature values with extensive calibration. We expect more observations will be available in the future, and these observations can serve as a reference for future model improvement.

To investigate the role of marsh on the adjacent waterbody, we implemented the coupled hydrodynamic, water quality, and marsh model for the York River Estuary. The unstructured grid generally follows the one used in the water quality study by Cai et al. (2020) with local refinements in the York River Estuary (Figure 4). The grid covers the whole Bay to accurately simulate the exchanges between the York River and the Bay. This grid contains 47,477 nodes and 73,433 elements. The grid system developed for this study uses flexible mesh, where rectangular elements are patched at deep channels while triangular elements are paved in the rest shoals and

**Table 1**  
Key Parameters of the Marsh Module

Parameter	Definition	Value	Unit
Fam	Fraction of production devoted to active metabolism	0.2	[-]
FPlf	Fraction of production routed to leaf biomass	0.6	[-]
FPst	Fraction of production routed to stem biomass	0.3	[-]
FPrt	Fraction of production routed to root biomass	0.1	[-]
$a^a$	Coefficients to transfer marsh biomass to canopy height	-0.0002	$\text{m}^3 \text{g}^{-1}$
$d^a$	Coefficients to transfer marsh biomass to canopy height	0.0036	$\text{m}^3 \text{g}^{-1}$
$e^a$	Coefficients to transfer marsh biomass to canopy height	0.054	m
crit <sup>a</sup>	Coefficients to transfer marsh biomass to canopy height	300	$\text{g m}^{-2}$
Acdw	Plant carbon-to-dry-weight ratio	0.38	$\text{g C g}^{-1} \text{DW}$
Pmbs	Coefficient for maximum growth rate function	0.4	$\text{g C g}^{-1} \text{DW day}^{-1}$
Topt	Optimal temperature for marsh production	27	$^{\circ}\text{C}$
KTg1	Effect of temperature below Topt on production	0.003	$^{\circ}\text{C}^{-2}$
KTg2	Effect of temperature above Topt on production	0.005	$^{\circ}\text{C}^{-2}$
ST <sup>b</sup>	Salinity choice and stress coefficient	35	PSU <sup>2</sup>
Saltopt <sup>b</sup>	Optimal salinity of this species	20, 12, 0	PSU
tinun <sup>b</sup>	Inundation pressure coefficient	0.2	[-]
$\alpha$	Initial slope of production versus irradiance curve	0.005	$\text{g C g}^{-1} \text{DW} \cdot (\text{E m}^{-2})^{-1}$
Ksh	Light attenuation by marsh	0.045	$\text{m}^2 \text{g}^{-1} \text{C}$
bmlf	Reference metabolism rate of leaf at reference temperature	0.01	$\text{day}^{-1}$
bmst	Reference metabolism rate of stem at reference temperature	0.01	$\text{day}^{-1}$
bmrt	Reference metabolism rate of root at reference temperature	0.01	$\text{day}^{-1}$
Tr	Reference temperature for leaf, stem, and root metabolism	20	$^{\circ}\text{C}$
KTb	Effect of temperature on leaf, stem, and root metabolism	0.08	$^{\circ}\text{C}^{-1}$
ad	Coefficients to calculate the seasonal mortality of leaf and stem	4	[-]
bd	Coefficients to calculate the seasonal mortality of leaf and stem	-4	$^{\circ}\text{C}^{-1}$
cd	Coefficients to calculate the seasonal mortality of leaf and stem	17	$^{\circ}\text{C}$
dd	Coefficients to calculate the seasonal mortality of leaf and stem	12.8	[-]
Anc	Marsh nitrogen to carbon ratio	0.01	$\text{g N g}^{-1} \text{C}$
Apc	Marsh phosphorus to carbon ratio	0.003	$\text{g P g}^{-1} \text{C}$
Aocr	Mass ratio of oxygen to carbon produced in photosynthesis	2.67	$\text{g DO g}^{-1} \text{C}$
FDO	Fraction of leaf and stem hydrolyzed in the upper layer of the sediment	0.5	[-]
FrtDO	Fraction of root metabolism as oxygen consumption	0.8	[-]
krh	Coefficient of DOC oxidation in the upper sediment layer	1	$\text{g m}^{-3}$

Note. The rest values are from Cerco and Moore (2001) and Cai (2018).

<sup>a</sup>Values are obtained based on model calibration of annual plant biomass. <sup>b</sup>Values are obtained based on model calibration of fresh and salt marsh.

tidal marshes. Outside the Bay, the grid resolution varies from 2.4 km for the continental shelf to 550 m at the Bay mouth. Inside the York River estuary, the along-channel grid resolution increases from 300 to 100 m from the mouth to the Pamunkey and Mattaponi Rivers. The cross-channel resolution increases from 200 m to less than 100 m upstream. The resolution is about 50 m in the area with extensive marshes (e.g., Sweet Hall Marsh). A hybrid shaved vertical grid system LSC<sup>2</sup> (Localized Sigma Coordinates with Shaved Cells; Zhang et al., 2016) is applied in this domain. There are up to 52 vertical layers in the deeper ocean and at least one layer in the shallow regions nearshore.

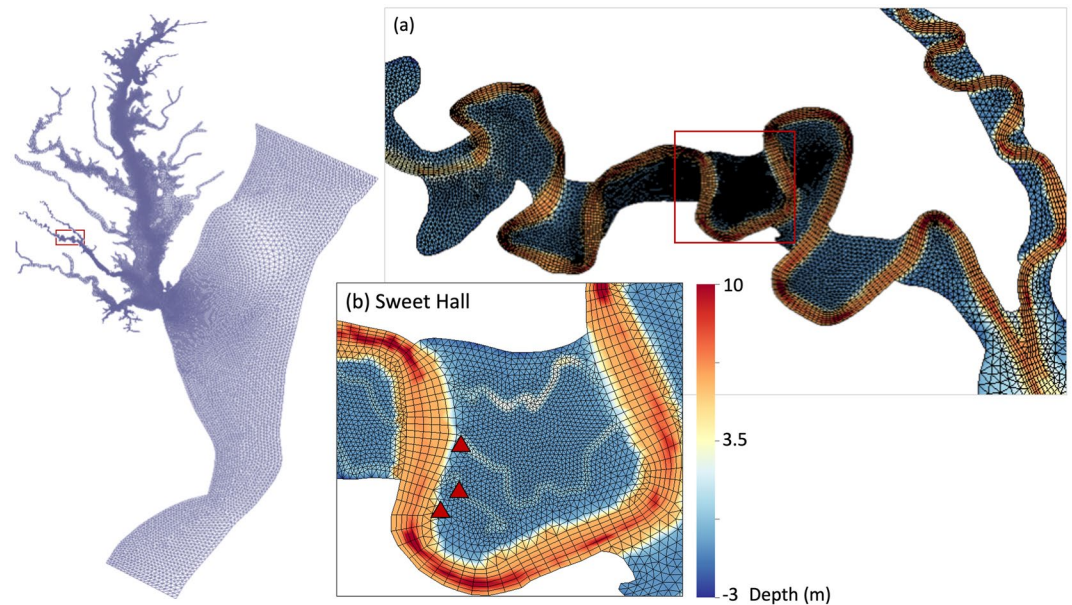


**Figure 4.** The SCHISM model domain with zooms on (a) the confluence section of the Pamunkey River and the Mattaponi River, (b) the Sweet Hall Marsh. Red triangles in panels (b) denote the sampling points of diurnal processes in this study.

The model simulation period is from 2010 to 2014 with a single non-split time step of 150 s. The open boundary is forced by elevation interpolated from two tidal gauges at Lewes, DE and Beaufort, NC. The temperature at the ocean boundary is nudged to HYCOM (<https://www.hycom.org>). The salinity is relaxed near the ocean boundary toward the World Ocean Atlas (<https://www.ncei.noaa.gov/products/world-ocean-atlas>) monthly climatological data. Hydrologic and nutrient loadings are from the outputs from the Phase 6 Watershed Model of the Chesapeake Bay Assessment Tool (CAST) (Shenk & Linker, 2013). The North American Regional Reanalysis provides the atmospheric forcing (Mesinger et al., 2006). The initial marsh biomass of all three marsh groups was set to be  $230 \text{ g C m}^{-2}$  (leaf  $100$ , stem, and root  $30 \text{ g C m}^{-2}$ , respectively) everywhere in the assigned marsh elements (Figure 1c). The model was spun up to equilibrate the water quality and marsh variables before simulating the target period of 2010–2014.

In addition to the calibrated setup (Base Scenario), we also conducted seven sensitivity tests to examine the responses of marsh and adjacent estuarine waters with different parameters or processes (Table 2). NV0 treats the marsh plants as plastic cylinders without any contributions to biochemical processes, that is, they only affect the local physical environments; in doing so, we can assess the ecological contributions from the hydrodynamic influence of the tidal marshes to the entire system. Tests #2 to #7 alter the parameters that are related to (a) marsh growth, (b) metabolism, and (c) uptake/release of nutrients, in the form of optimal temperature for marsh

**Table 2**  
*List of the Sensitivity Tests*

Sensitivity test abbreviation	Sensitivity test name	Changed parameters
NV0	Marsh biological functions disabled (i.e., with only physical effects)	
GM1	High growth rate and metabolism rate	$P_{\text{mbs}} = 0.6 \text{ g C g}^{-1} \text{ DW day}^{-1}$ $\text{bmlf} = \text{bmst} = \text{bmrt} = 0.015 \text{ day}^{-1}$
GM2	Low growth rate and metabolism rate	$P_{\text{mbs}} = 0.3 \text{ g C g}^{-1} \text{ DW day}^{-1}$ $\text{bmlf} = \text{bmst} = \text{bmrt} = 0.0075 \text{ day}^{-1}$
TG1	High optimal temperature for leaf growth	$T_{\text{opt}} = 32 \text{ }^{\circ}\text{C}$
TG2	Low optimal temperature for leaf growth	$T_{\text{opt}} = 22 \text{ }^{\circ}\text{C}$
NP1	High nitrogen/phosphorus-to-carbon ratio	$\text{Anc} = 0.02$ ; $\text{Apc} = 0.006$
NP2	Low nitrogen/phosphorus-to-carbon ratio	$\text{Anc} = 0.005$ ; $\text{Apc} = 0.0015$

production ( $Topt$ ), coefficients for maximum growth rate function ( $Pmbs$ ), reference metabolism rates at reference temperatures ( $bmlf$ ,  $bmst$ , and  $bmrt$ ), and marsh nitrogen or phosphorus to carbon ratios ( $Anc$  and  $Apc$ ), respectively. All the sensitivity tests use the identical physical setup as the Base Scenario.

## 2.4. Analysis Methods

### 2.4.1. Skill Assessment

To assess the model skill, model simulations of various water quality state variables are compared with CBP observations in the York, Pamunkey, and Mattaponi Rivers. Root mean square error (RMSE), correlation coefficient (CC), and relative error (RE) of model simulations against observations in both water surface and bottom are calculated to evaluate the model performance. The RMSEs of the 3-month moving averages (December to February, March to May, June to August, and September to November) at the CBP stations are calculated for the seasonal quantitative assessment. In addition to the use of statistics, we also use times series comparisons at selected stations in the Pamunkey River, West Point, and lower York River to assess the model skills. In addition, we compare the mean modeled tidal range along the York River channel against the observations to ensure the tidal flooding in the marshes is correctly simulated in terms of frequency and duration. The mean tidal range is estimated as the difference between modeled high tide and low tide over a tidal cycle averaged over the entire simulation period (the model output frequency is every 30 min). Furthermore, we performed harmonic analysis on the modeled elevation and observed water depth at VECOS stations WH and SH to further analyze the model skills (Pawlowicz et al., 2002).

### 2.4.2. Marsh Biomass and Productivity

For the simulation of marsh biomass, due to the lack of continuous, in situ measurement of tidal freshwater marsh biomass in the York River Estuary (e.g., Sweet Hall Marsh), we compared the modeled marsh biomass with a few historical observations (Davies, 2004; Perry & Hershner, 1999) as a qualitative evaluation. The marsh net productivity is calculated by:

$$MPP = \sum_{m=1,2,3} (Plf_m \cdot (1 - Fam_m) - MTlf_m \cdot BMlf_m) \cdot LF_m - MTst_m \cdot BMst_m \cdot ST_m - BMrt_m \cdot RT_m \quad (33)$$

where  $m$  is the index of the three tidal marsh groups (salt marsh, brackish marsh, and freshwater marsh).

### 2.4.3. Phytoplankton Production

Local phytoplankton production in each grid cell is computed by integrating the local phytoplankton production in the water column:

$$GPP = \sum_{i=1}^n (C1_i \cdot G1_i + C2_i \cdot G2_i + C3_i \cdot G3_i) \cdot dep_i \quad (34)$$

where GPP is areal gross primary production of phytoplankton ( $g C m^{-2} day^{-1}$ ),  $n$  is the number of vertical layers in each element,  $i$  is the vertical layer index,  $C1$ ,  $C2$ ,  $C3$  are carbon-based phytoplankton biomass of three groups (diatoms, green algae, and cyanobacteria) over each layer, respectively ( $g C m^{-3}$ ),  $G1$ ,  $G2$ ,  $G3$  are growth rates of the three phytoplankton groups ( $g C g C^{-1} day^{-1}$ ), respectively, and  $dep$  is layer thickness ( $m$ ).  $G1$ ,  $G2$ ,  $G3$  are determined by the local temperature and other factors that limit algal growth (Cercu & Noel, 2017). The calculated spatially varying GPP is averaged with the weight of element area for the entire York River Estuary in each scenario and sensitivity test.

### 2.4.4. Material Fluxes

Annual-averaged net material fluxes were calculated along the 11 transects from the upstream to the downstream to study the role of the marshes (Figure 1bc). Net fluxes of dissolved organic carbon (DOC) and inorganic nutrients (dissolved inorganic nitrogen, DIN, and phosphate,  $PO_4^{3-}$ ) were analyzed in the Base Scenario and all the sensitivity tests. The net flux is the difference between outflux (marked as positive toward the mouth of the York River) and influx (marked as negative), both of which are calculated as the sectionally integrated product of the flow velocity normal to the transect and the concentrations of materials:

$$\text{net flux} = \text{outflux} - \text{influx} = \int_A (u_n \cdot \text{Var}) dA \quad (35)$$

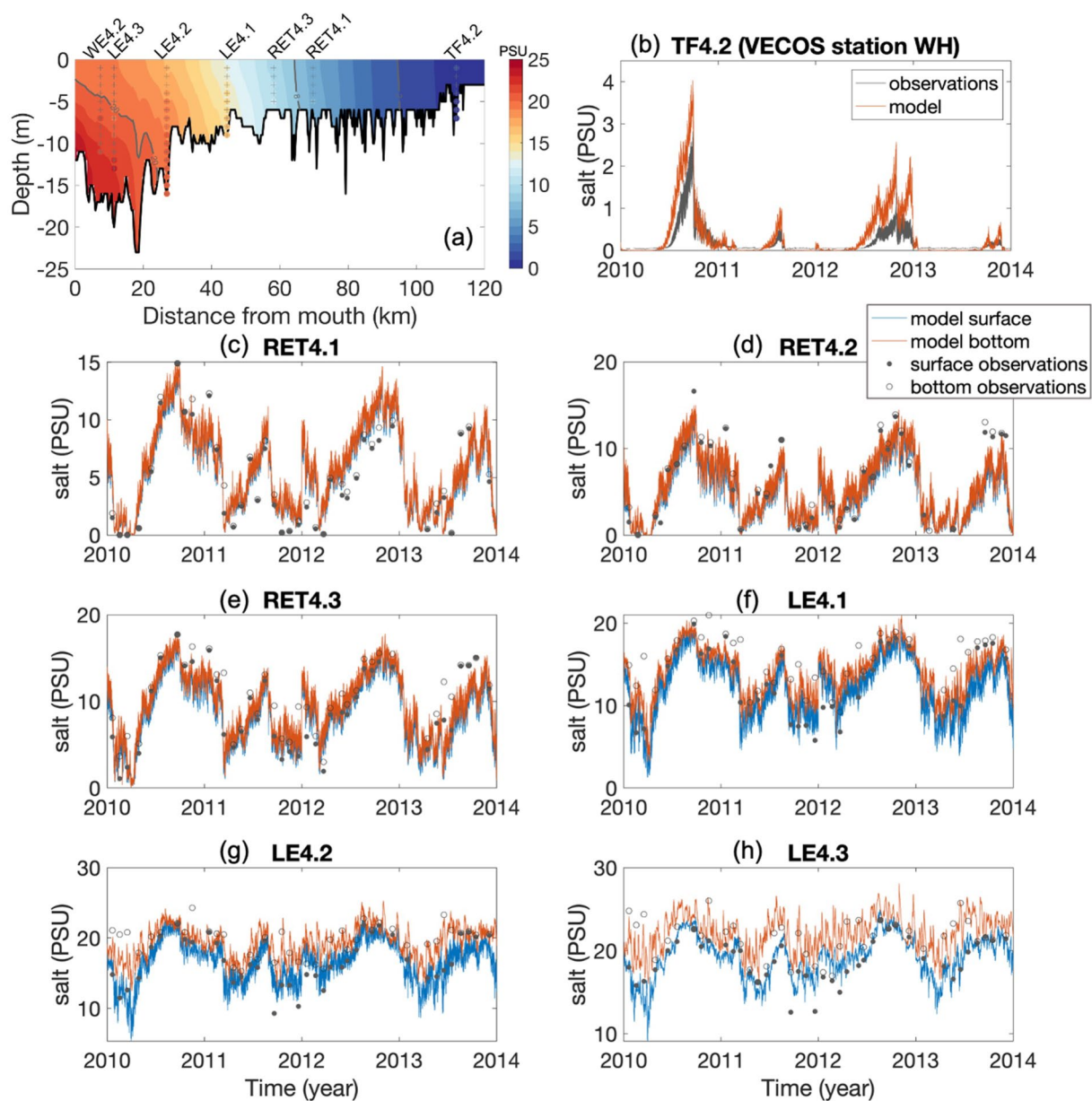


**Figure 5.** (a) Four-year averages of salinity along the York-Pamunkey River channel as shown in Figure 1. The colored contours represent model results; the colored circles with gray “+” represent the observations from the Chesapeake Bay Program (CBP). (b–h) Time series of observed and modeled salinity at York River Estuary stations from upper stream to the mouth. (b) In station TF 4.2, the gray line denotes the high frequent observations from Virginia Estuarine and Coastal Observing System (VECOS) and the red line represents the modeled bottom salinity. (c–h) In the remaining stations, gray dots and circles denote CBP observations. Blue lines represent the surface modeled salinity and red lines represent the bottom salinity.

where  $u_n$  is the normal velocity ( $\text{m s}^{-1}$ ),  $\text{Var}$  is the concentration of DOC or other nutrients,  $A$  is the vertical area of the transect ( $\text{m}^2$ ).

### 3. Model Assessments

#### 3.1. Physical Environments

CBP and VECOS stations along the channel of the York River are used to evaluate the model skills of salinity (Figure 5). In Figure 5a, the 4-year averaged observed salinities are represented by colored circles with light gray crosses inside. As evidenced by the fact that most of the circles completely disappear into the background

**Table 3**  
*Skill Assessment (Root Mean Square Error (RMSE), Correlation Coefficient (CC), and Relative Error (RE)) for Model-Data Comparisons of Certain Water Quality Station Variables From 2010 to 2014*

Region	Station	Index	Layer	Salinity	Chl-a	DO	DIN	PO <sub>4</sub> <sup>3+</sup>
Pamunkey	TF4.2	RMSE	S	0.54	8.09	2.73	0.14	0.03
	TF4.2	RMSE	B	0.53	/	2.86	0.15	0.03
	TF4.2	CC	S	0.90	0.22	0.85	0.76	-0.29
	TF4.2	CC	B	0.81	/	0.84	0.74	-0.29
	TF4.2	RE (%)	S	35.21	12.80	9.92	18.19	26.92
	TF4.2	RE (%)	B	50.38	/	14.79	18.35	37.28
	RET4.1	RMSE	S	2.15	7.75	1.45	0.14	0.04
	RET4.1	RMSE	B	2.19	/	1.58	0.14	0.04
	RET4.1	CC	S	0.86	0.18	0.92	0.60	0.50
	RET4.1	CC	B	0.85	/	0.91	0.61	0.50
	RET4.1	RE (%)	S	11.55	19.98	9.29	43.33	46.12
	RET4.1	RE (%)	B	8.13	/	10.84	45.24	44.91
Mattaponi	TF4.4	RMSE	S	/	5.35	3.54	0.15	0.06
	TF4.4	RMSE	B	/	/	3.65	0.14	0.06
	TF4.4	CC	S	/	0.21	0.80	0.28	0.13
	TF4.4	CC	B	/	/	0.80	0.27	0.14
	TF4.4	RE (%)	S	/	59.76	23.44	4.49	46.05
	TF4.4	RE (%)	B	/	/	27.58	1.46	53.98
	RET4.2	RMSE	S	2.91	7.85	2.17	0.12	0.03
	RET4.2	RMSE	B	2.75	/	2.08	0.12	0.03
	RET4.2	CC	S	0.84	0.23	0.84	0.61	0.56
	RET4.2	CC	B	0.82	/	0.85	0.55	0.54
	RET4.2	RE (%)	S	19.15	15.74	5.50	13.47	24.26
	RET4.2	RE (%)	B	14.28	/	5.65	16.09	25.93
York	RET4.3	RMSE	S	2.34	25.15	1.80	0.11	0.03
	RET4.3	RMSE	B	2.93	/	2.25	0.12	0.03
	RET4.3	CC	S	0.88	-0.10	0.88	0.67	0.75
	RET4.3	CC	B	0.79	/	0.85	0.46	0.77
	RET4.3	RE (%)	S	9.08	50.67	14.69	54.57	34.62
	RET4.3	RE (%)	B	15.26	/	22.24	57.41	31.67
	LE4.1	RMSE	S	1.81	14.11	1.67	0.10	0.03
	LE4.1	RMSE	B	2.71	/	2.37	0.10	0.04
	LE4.1	CC	S	0.93	-0.20	0.93	0.22	0.73
	LE4.1	CC	B	0.76	/	0.90	-0.14	0.76
	LE4.1	RE (%)	S	7.08	31.80	16.88	52.61	27.85
	LE4.1	RE (%)	B	11.90	/	28.26	52.16	34.25
LE4.2	RMSE	S	1.65	4.21	1.44	0.09	0.03	
LE4.2	RMSE	B	1.44	/	1.53	0.08	0.02	
LE4.2	CC	S	0.89	0.27	0.95	-0.10	0.70	
LE4.2	CC	B	0.77	/	0.92	0.03	0.70	

**Table 3**  
*Continued*

Region	Station	Index	Layer	Salinity	Chl-a	DO	DIN	PO <sub>4</sub> <sup>3+</sup>
	LE4.2	RE (%)	S	2.55	4.04	14.58	45.69	22.04
	LE4.2	RE (%)	B	1.50	/	16.26	13.90	20.94

*Note.* Model outputs are interpolated onto the corresponding observation times (insufficient number of observations is denoted by “/”).

in Figure 5a, the overall average RMSE of salinity in the York River Estuary stations is 1.81 PSU at the surface and 2.05 PSU at the bottom (Table 3). In addition, the mean seasonal RMSE of salinity at all the stations is 2.07 PSU at the surface and 2.37 PSU at the bottom. Particularly, the RMSE of the high-salinity season is 1.96 PSU at the surface and 1.73 PSU at the bottom. The model captures the saltwater intrusion events well in terms of occurrence, duration, and salinity magnitude (Figure 5b). The error in salinity is less than 0.8 PSU at Station TF4.2 (White House). In addition, the model captures well the stratification in the lower York River (Figures 5f–5h).

In the York River Estuary, the high-frequency data of total water depth at two VECOS stations and the historic tidal range from the NOAA tide tables are used to evaluate the model skills for the tidal range (Cai, Qin, et al., 2022; Cai, Shen, et al., 2022). The modeled tidal range agrees with the historic observations along the York River and captures its along-channel variability, with an RMSE of 4.69 cm (Cai, Qin, et al., 2022; Cai, Shen, et al., 2022). The model tends to overestimate the tidal range at the mouth of the York River while underestimating at the upper end of the Pamunkey and Mattaponi. The largest difference in the tidal range is 7.98 cm at the station of Northbury, in the Pamunkey River. Since the historical data were measured a long time ago, changes in bathymetry in the York River could be expected. Harmonic analysis shows that the major constituents are well modeled in terms of phases and amplitudes (Cai, Qin, et al., 2022; Cai, Shen, et al., 2022). The model results slightly overestimate the M2 amplitudes by 1.36 cm at Station Sweet Hall and 2.31 cm at Station White House. Overall, the model performance on tidal simulation is satisfactory.

### 3.2. Water Quality Variables

Overall, the model captures the seasonal cycles and interannual variability of chlorophyll-a, DO, DIN, and PO<sub>4</sub><sup>3-</sup> (Figure 6). Model skill statistics for these variables are presented in Table 3 and summarized in target diagrams (Figure 6ef). The model successfully simulates the chlorophyll-a concentrations in the Pamunkey and York Rivers, but the model slightly underpredicts the peak chlorophyll-a concentrations at West Point. DO is reasonably predicted with a high CC (larger than 0.80), a small RE (mostly less than 25%), and a low normalized RMSE for all the York stations (Table 3). The simulated DIN generally follows the observed pattern of high spring concentrations and low summer/fall concentrations. The magnitude is captured with a relatively small RMSE (0.12 g m<sup>-3</sup> on average), though it is underestimated by the model in the fall of 2013 when the observed DIN is higher than the other years. Phosphate is also well simulated by this model and shows the typical seasonal pattern that the concentration is low in spring and high in summer and fall.

### 3.3. Tidal Marshes

Overall, the model results for marsh biomass and productivity show a qualitatively reasonable seasonal pattern (Figures 7a–7e). The high biomass is around 600 g C m<sup>-2</sup>, which is in the same range as the measured range of 490–800 g C m<sup>-2</sup> (Davies, 2004; Perry & Hershner, 1999). In Sweet Hall Marsh, marsh biomass tends to be relatively low at marsh edges where the inundation stress is high and tends to increase toward landward locations where the inundation stress is reduced (Figure 7f). With the identical initial distribution of marsh biomass among the three groups, the distribution of marsh species and biomass after equilibrium is generally consistent with the spatial pattern of the observed local community structure (Mitchell et al., 2017). The group of freshwater marshes, which prefer low salinity, has lower biomass toward the West Point where higher salinity occurs (Figure 7e), and it takes up the majority of the tidal marshes in the study area. Spring and summer are dominated by marsh growth, while respiration and mortality are larger than production in fall and winter (Figure 7c). The tidal freshwater marsh in Sweet Hall receives greater salinity stress in high-salinity seasons (i.e., summer and

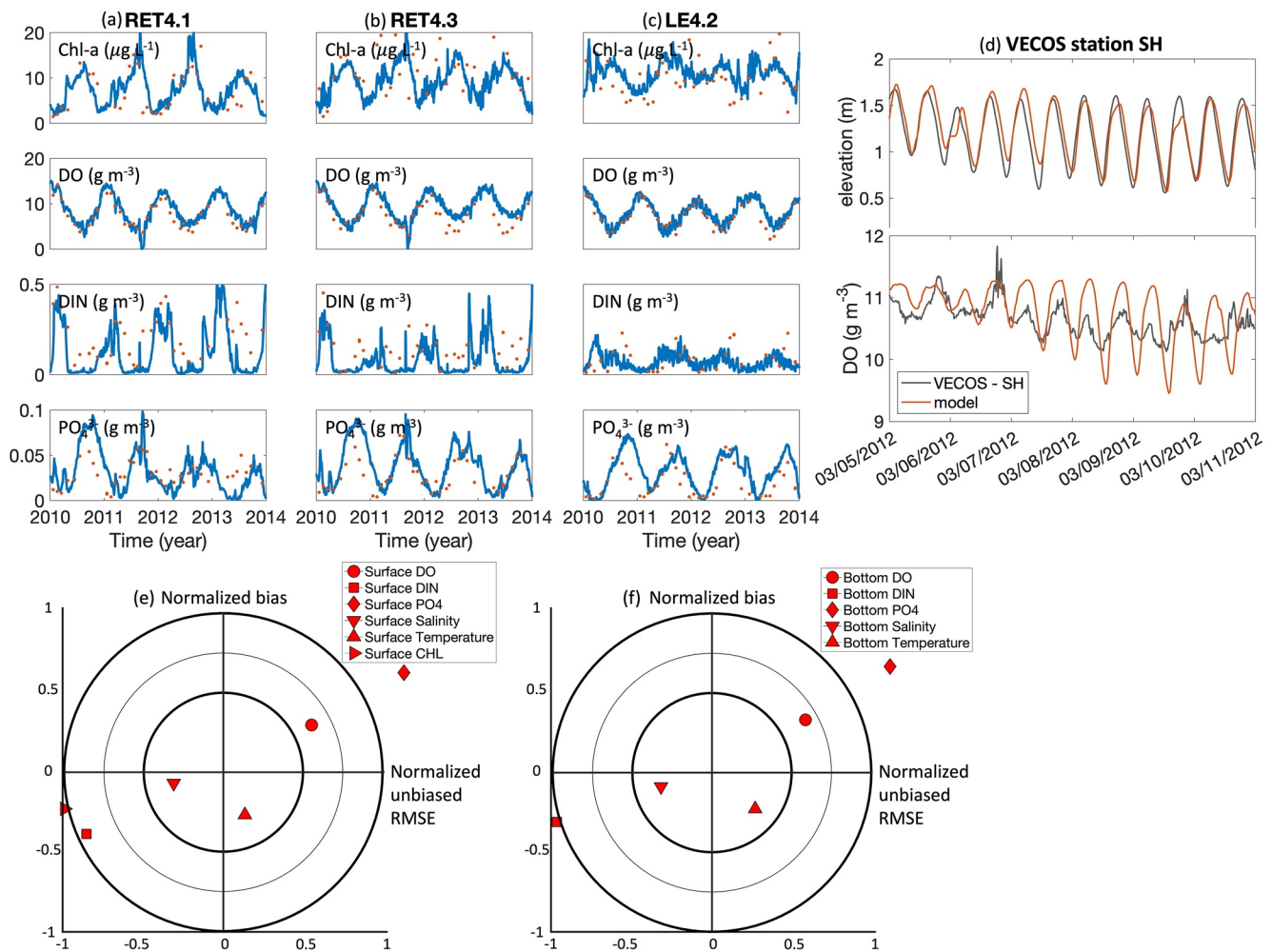


**Figure 6.** (a–c) Comparisons of model-simulated (blue lines) and observed (red dots) water properties at three stations along the channel of the Pamunkey to the York River, including surface chlorophyll-a, bottom DO, DIN, and PO<sub>4</sub><sup>3-</sup>. (d) Comparisons of model-simulated (red lines) and observed (gray lines) high-frequency elevation and bottom DO at VECOS station SH. (e, f) Target diagram for DO, DIN, phosphate, salinity, temperature, and surface chlorophyll-a at all CBP stations with sufficient observations (RET4.1, RET4.2, RET4.3, LE4.2, and LE4.2). Station locations are denoted in Figure 1a.

fall). The shading effect is stronger in summer when marsh biomass is higher. Marsh growth received increased inundation stress in fall and winter, but the difference is minor.

We also tested the responses of marsh biomass to different parameter sets (Figure 8). Because marsh growth mainly depends on light and temperature, while salinity and tidal range do not change much in the sensitivity tests, the simulated marsh biomass is mainly sensitive to model dynamic parameters (e.g., *Topt*, *Pmbs*, *bm1f*, *bmst*, and *bmrt*). An increase of 50% in both growth rate and metabolism rate causes a 29.52% reduction in the mean biomass, while a 25% decrease in the two rates increases the mean biomass by 24.97%. An increase or decrease of 5°C in the optimal temperature of the leaf growth decreases or increases the mean biomass by 6.26% and 3.55%, respectively. On the other hand, changes in carbon to nitrogen or phosphorus ratio (*Anc* and *Apc*) have little impact on marsh biomass (e.g., variations are <0.24%).

## 4. Discussion

### 4.1. Impacts of Marsh on Oxygen Dynamics and Organic Carbon

DO below saturation level has been observed in the water body adjacent to the marshes. In the Pamunkey River, the loss of DO due to marsh is estimated to be about 1.12–2.77 g m<sup>-2</sup> day<sup>-1</sup> (Cercio & Noel, 2017). To test the effects of marsh on DO, we compared model simulations of the Base Scenario (with marsh) and NV0 (without

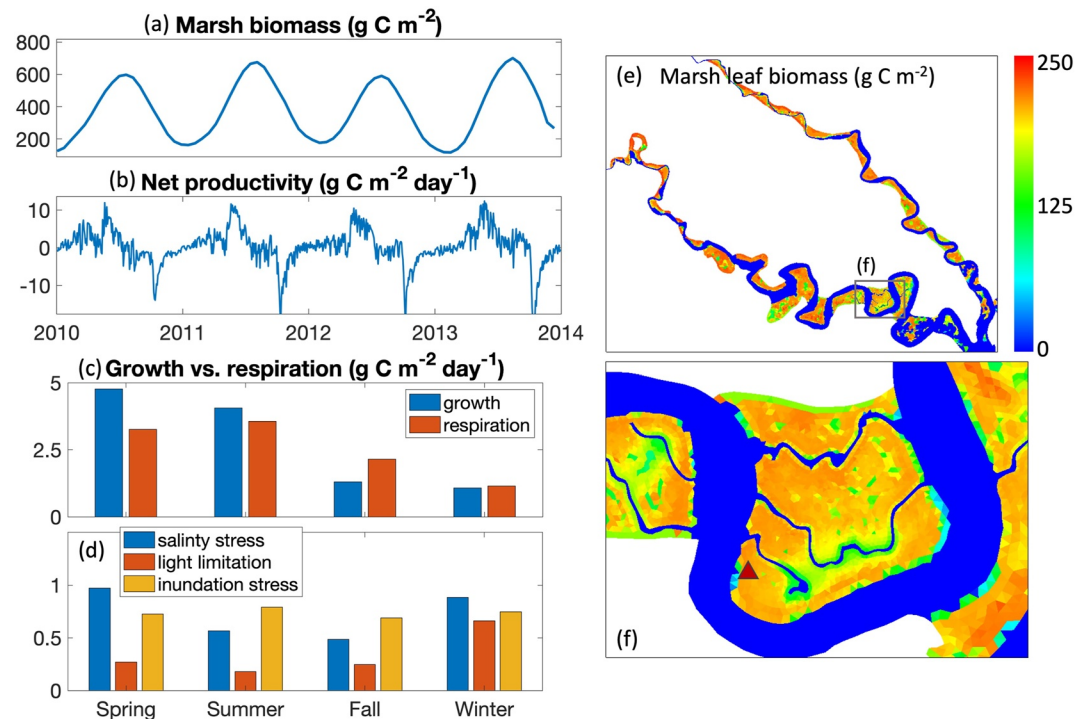


**Figure 7.** (a, b) Spatial averages of marsh biomass (including leaf, stem, and root) and net marsh productivity in Sweet Hall Marsh. (c) Seasonal leaf growth versus respiration of the tidal freshwater marsh in the Sweet Hall sampling station which is denoted by red triangle in (f). (d) Seasonal variations of the limitation functions of the tidal freshwater marsh in the same sampling station as (c). (e) Spatial distribution of tidal freshwater marsh leaf biomass in the York River Estuary in summer, and (f) Zoom-in of the Sweet Hall Marsh.

marsh). If the biological function of the marsh is removed, the spatial pattern of the annually averaged bottom DO in NV0 (red line in Figure 9b) is closer to saturation in the shallow water of the upstream, as expected. However, the Base Scenario (blue line in Figure 9b) shows that the existence of a highly productive marsh, which drives more heterotrophic respiration, tends to decrease the bottom oxygen concentrations along with a higher level of DOC in the system (Figure 9bc). The suggested high pelagic respiration is also supported by experiments in other systems (Koch & Gobler, 2009). Compared with NV0, the existence of the marshes not only lowers the overall bottom DO level but also enhances the diurnal swing of DO inside and adjacent to the marshes (Figure 10b). During low tide, the DO concentration sometimes drops to below  $2 \text{ g m}^{-3}$ , accompanied by the export of high DOC and oxygen demand (e.g., sulfide) from the anaerobic marsh sediments (Figure 10ab-3). The outflow of

low-DO water further drives the swing in the creeks and channels. The drop in DO concentration during low tide is consistent with observations in other systems such as Jug Bay in Maryland (Swarth & Peters, 1993), Elkhorn Slough (Nidzieko et al., 2014), and Lower South San Francisco Bay (Roberts et al., 2022) in California.

The highly productive marshes tend to be significant sources of organic carbon for the York River Estuary. Marshes from Horseshoe in the upstream Pamunkey River to the West Point contribute about 60%–75% of the annual net flux of DOC near the West Point (Figure 11a). As a result, the overall DOC concentration decreased significantly in the York River Estuary in the sensitivity test NV0, especially in the Pamunkey River (about 80%) once the extensive marshes were removed (Figure 9c). In other sensitivity tests, the changes in both the DOC concentration and DOC net fluxes are relatively minor (Figure 12a for the net fluxes at West Point, fluxes at other interfaces, and concentrations are not shown). The major reason for the minor changes in the DOC and DOC fluxes is that marsh biomass does not change much in

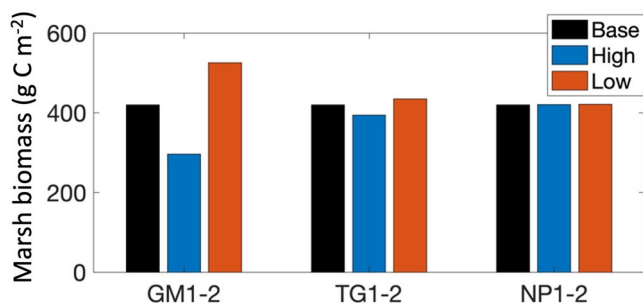


**Figure 8.** Response of annually-averaged tidal freshwater marsh biomass ( $\text{g C m}^{-2}$ ) in the Sweet Hall Marsh to sensitivity tests listed in Table 2 (GM1,2, TG1,2, and NP1,2). “High” denotes the changed parameters are larger than the Base Scenario and “Low” indicates the modified parameters are smaller than the original values.

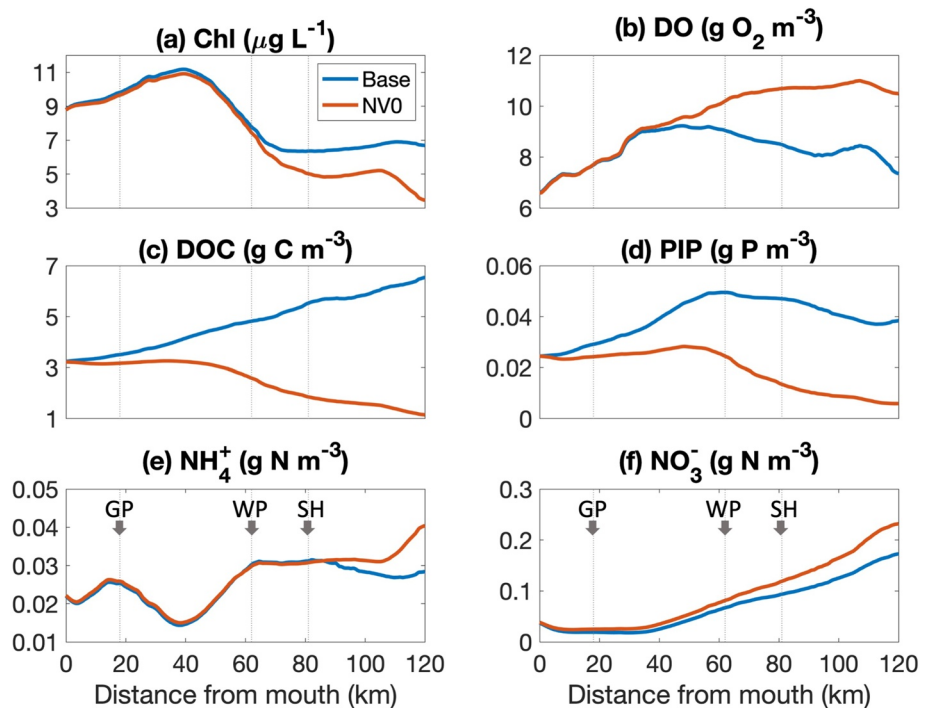


**Figure 9.** Comparisons of Base Scenario and selected sensitivity tests (NV0) on the annual mean values of bottom DO and other surface water properties, including chlorophyll-a, ammonia, nitrate and nitrite, phosphate, and dissolved organic carbon, along the channel of the Pamunkey and the York Rivers. The along-channel transect is denoted in Figure 1a. Locations of Gloucester Point (GP, CBNEER/VECOS station YB in Figure 1a), West Point (WP, CBP station RET 4.3), and Sweet Hall (SH) are denoted in panels (e, f) along with gray dotted lines.

these sensitivity tests except for GM1 and GM2 (Figure 8). For example, in NP1, and NP2, the marsh biomass changes by less than 0.24%, and the DOC net fluxes change by less than 0.8%. Although marsh biomass changes up to about 30% in GM1 and GM2, the changes in net DOC outfluxes are less than 7% due to a compensating effect from carbon settling and release in the lower layer. Because of the presence of marsh, the surface chlorophyll-a concentration is also higher in the Base Scenario compared to NV0. Although the higher chlorophyll-a concentration ( $<2 \mu\text{g L}^{-1}$ ) also contributes to the higher DOC level ( $<0.12 \text{ g m}^{-3}$ ), this contribution is much smaller than the DOC change caused by marsh (about  $3 \text{ g m}^{-3}$ ; Figure 9c). Thus, the model results suggest that the dominant contributor to DOC changes is not phytoplankton but tidal marshes. Qin and Shen (2019) show that ecosystem gross primary production (GPP) is several times larger than the pelagic GPP in the Pamunkey River, suggesting a high contribution from the tidal marshes, which is consistent with this model estimations. There are limited available DOC observations, and synthesis of observed DOC fluxes on an estuary scale is still lacking. According to the limited DOC observations in the York River Estuary, the DOC concentrations range from 3 to  $6 \text{ g m}^{-3}$ , which agrees with our model results. However, large variations of DOC exchanges between the marshes and the adjacent water in the channels have been observed at different sites and times (Bukaveckas, 2021; Czaplá et al., 2020; Neubauer & Anderson, 2003). These observations suggest that marshes may either be a source or a sink to DOC at different locations on the local scale.

In addition, this model performs well in simulating DO against measurement in the adjacent channel, suggesting the model's biochemical processes function correctly to simulate the low DO. Our model configuration suggests that a large portion of DO is consumed by the DOC in the marsh. This is consistent with some existing marsh models in the literature that simply add a DO sink term to include marsh respiration with an appropriate respiration rate based on observed values in the Pamunkey River and other marshes (Cercó & Noel, 2017).

#### 4.2. Impacts of Marsh on Nitrogen and Phosphorus

Overall, tidal marshes tend to be a nutrient modifier (Figures 9d–9f). In this modeling study, the marsh functions as a sink of nutrients directly through the settling of organics from fallen leaves or other tissues and

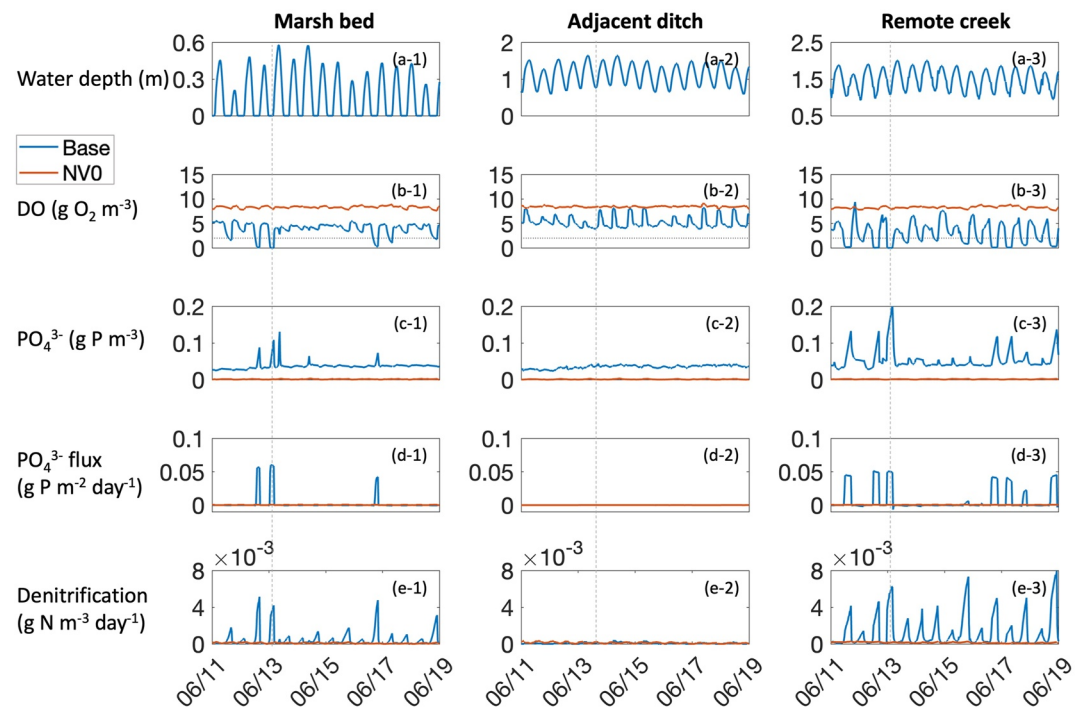


**Figure 10.** Zoom-in of a 9-day window of the simulated water properties (a) water depth, (b) dissolved oxygen, (c) phosphate, (d) sediment phosphate flux, and (e) denitrification at three sampling stations in the Sweet Hall in Base and NV0 (marsh removal) scenarios. The three sampling stations are denoted in Figures 4b and 4c. The gray dotted horizontal line in (b) denotes a dissolved oxygen concentration of  $2 \text{ g m}^{-3}$ . Gray dotted vertical lines denote a moment of low tide along with low-DO events.

particulates transported to the marshes, as observed in various tidal marsh systems (DeLaune et al., 1981). The sediment mineralization processes can enhance denitrification to release nitrogen gas, which is consistent with field measurements and other estimations (Anderson et al., 1997; Axelrad et al., 1976; Bowden, 1986; Koch & Gobler, 2009). Given the larger form drag from the marsh plants than the estuarine water, tidal marshes trap the particulate nutrients quickly and incorporate them into the sediment layer. This helps reduce nutrient loading into the open water. However, diel DO variations occur in the tidal marshes and adjacent channels. The low-DO events in these diel cycles enhance bottom phosphate release and denitrification. For example, when the bottom DO concentration drops below  $2 \text{ g m}^{-3}$  at low tide (Figure 10b), a pulse of the bottom release of phosphate occurs (Figure 10d), which largely increases the phosphate concentration (Figure 10c). As a result, the phosphate concentration is lower in the sensitivity test NV0 than in the Base Scenario (Figure 9d) and the net phosphate flux from the upstream decreases significantly in NV0 (Figure 11c). On the other hand, the diel bottom DO in the Base Scenario prompts more denitrification (Figure 9e), while there is more DIN retained in the system in the sensitivity test NV0 (Figures 9e and 9f). The presence of marsh reduces net DIN fluxes into the York River at West Point by about 10.5% (Figure 11b).

According to the sensitivity tests, changes in marsh growth rate, metabolism rate, and optimal growth temperature have little impact on net fluxes of inorganic nutrients from the upstream to the lower stream at the West Point (e.g., <7%, Figure 12b c-2), while the trend of nutrient impacts from the marsh is consistent with field measurements and experiments in multiple systems (e.g., Anderson et al., 1997; Axelrad et al., 1976; Bowden, 1986; Feijtel et al., 1985; Jordan et al., 1983; Koch & Gobler, 2009). When the carbon to phosphorus ratio is increased by 100%, the  $\text{PO}_4^{3-}$  fluxes are reduced by 32.0%. On the other hand, decreasing these ratios by 50% increases the flux of  $\text{PO}_4^{3-}$  by 6.6%. The changes in  $\text{PO}_4^{3-}$  and DIN outfluxes are generally proportional to each other with a negative linear relationship (Figure 12e). For example, in the sensitivity test of GM1, the change in DIN outfluxes is negative while the changes in DOC and  $\text{PO}_4^{3-}$  fluxes are positive because lower DO due to higher DOC prompts more denitrification to remove DIN from the system.

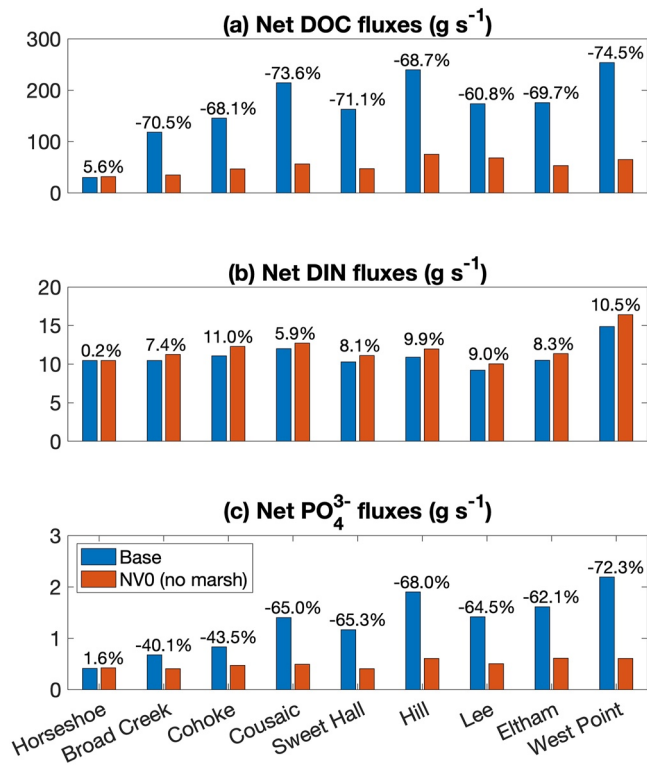


**Figure 11.** Net fluxes of (a) dissolved organic carbon, (b) dissolved inorganic nitrogen, and (c) total inorganic phosphate from the upper stream of Pamunkey River to the downstream in the Base Scenario and sensitivity test NV0. Locations of these cross-sections are denoted in Figures 1b and 1c. The percentage denoted in each panel equals  $(NV0 - \text{Base}) / \text{Base} \times 100\%$ . In these cross-sections, the influx (negative) refers to the direction from the river mouth to the upper streams and the outflux (positive) refers to the direction from the upper stream to downstream.

### 4.3. Impacts of Marsh on Chlorophyll-A and Phytoplankton Productions

The impacts of tidal marshes on the ecosystem, including the phytoplankton dynamics, result from a combination of physical and biological factors. In this study, the physical functions of tidal marshes were kept identical, and only the biological impacts of marshes were investigated based on different scenarios and sensitivity tests. The major biological impact of the marsh on adjacent water quality is nutrient availability. The marsh tends to enhance the growth of phytoplankton by providing a substantial source of nutrients, and this is consistent with experiments in other systems (e.g., Long Island, New York; Koch & Gobler, 2009). The chlorophyll-a concentration in the upstream region above West Point tends to slightly decrease in the sensitivity test NV0 compared to the Base Scenario (Figure 9a). Along with the decreased chlorophyll-a in NV0, phytoplankton production (PP) in the York River Estuary decreases by 3.1% (Figure 12d). The change in the PP is positively correlated to the changes in the  $PO_4^{3-}$  net fluxes from the upstream through West Point (Figure 12g). Although the change in the PP has a significant linear relationship with the change in the DIN, the correlation is negative (Figure 12f). Therefore, PP is more limited by the availability of phosphate than DIN. However, the change in PP (3.1%) is much smaller in magnitude than the change in phosphate (72.3%), which indicates that the phytoplankton dynamic in the York River Estuary is mostly dominated by flushing and light limitations (Sin et al., 1999).

### 4.4. Uncertainties and Limitations

In this study, we focused on the development and implementation of a new marsh model. This marsh model is embedded in a 3D hydrodynamic water quality model and is used to simulate the impacts of the marsh on estuarine biochemical processes in the York River Estuary. This model is developed based on current understanding and available data with a few assumptions.

For example, low-DO events have been observed near tidal marshes, but the mechanism is not fully understood. The low-DO events could be caused by the increased heterotrophic respiration driven by the DOC fluxes from the marshes or oxygen demand from the sediment of the tidal marshes (e.g., diffused sulfide). The material that is exported from the tidal marshes has been observed to be dominated by organic carbon or inorganic carbon at different times or locations (Chen et al., 2022; Czapla et al., 2020; Feijtel et al., 1985; Jordan et al., 1983; Knobloch et al., 2021; Koch & Gobler, 2009; Tzortziou et al., 2011). Currently, the marsh model in this study allows both exports of organic carbon and low sediment redox potential that consumes oxygen demand to fit the observations. However, the knowledge gaps about the low-DO mechanism and a lack of sufficient observations in marsh-relevant processes need to be further explored. In addition, a few simplifications were applied to the model implementations. For example, we did not include the simulations of the SAV in this study due to their much smaller footprints than the tidal marshes in this system, especially upstream (Moore, 2009). Also, the uncertainty of the bathymetry data makes it difficult to delineate the habitats of tidal marshes or SAV. In addition, this model does not include the small sub-tributaries of the York River Estuary, leaving out approximately 35% of the tidal marshes in the entire York River watershed, the majority of which are embayed in the sub-tributaries that must be highly resolved and require more computational resources. Due to the lack of observational data on marsh biomass and other fluxes between different interfaces, our model might need further calibration, even though the current simulation results are supported by relevant studies and field measurements. Sedimentation and the evolution of marsh platforms were not included because of the relatively short (seasonal and annual) time scale, but their effects on biochemical processes can be substantial over a longer time scale (DeLaune et al., 1981; Hatton et al., 1982); in addition, the morphological feedback to physical processes will be significant, particularly if the marsh extent changes significantly, as implied by the tidal range results shown in Cai, Qin, et al. (2022), Cai, Shen, et al. (2022). Overall, our study here provides a successful first

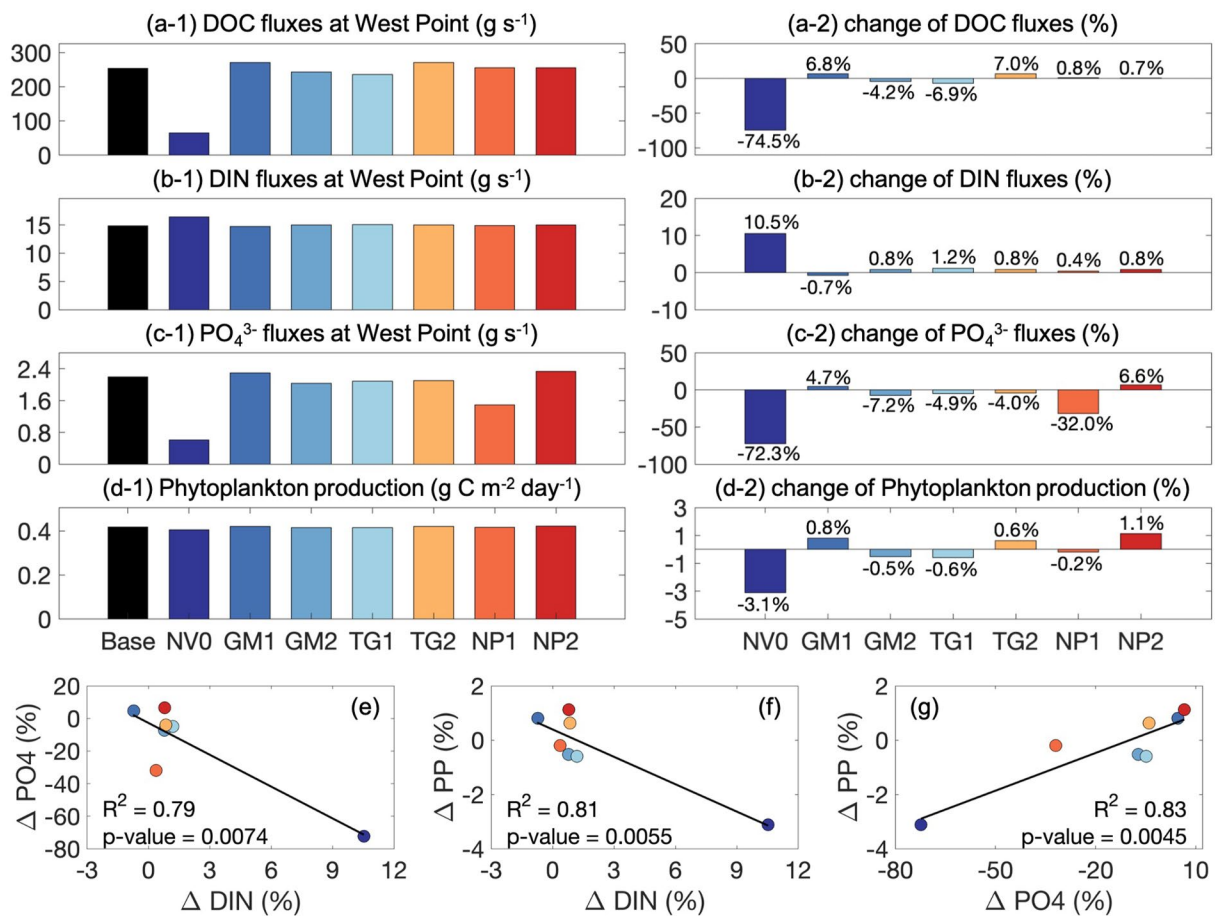


**Figure 12.** (a–c) Net nutrient fluxes from the West Point to the York River and (d) spatially averaged phytoplankton production in the York River Estuary in Base Scenario and sensitivity tests. (e–g) Linear regressions between the changes of DIN fluxes, PO<sub>4</sub><sup>3-</sup> fluxes, and the estuary phytoplankton production as shown in (b–d). The colors of the points in (e–g) correspond to those in (a, b) for each sensitivity test.

implementation of the marsh model to study the role of tidal marshes on estuarine biochemical processes under complex wetting and drying environments.

## 5. Conclusions

We developed a new marsh model inside the framework of a 3D unstructured-grid hydrodynamic water quality model (SCHISM-ICM-Marsh) to study the roles of tidal marshes on estuarine biochemical processes in the York River Estuary. This model showed good performance in simulating the physiological processes of tidal marshes, the wetting-drying physical processes, and the interplay among water quality properties such as chlorophyll-a, DO, and other nutrients. The model results demonstrated that the tidal marshes drive the local diurnal swings of water column oxygen by adding the sediment oxygen demand and exporting dissolved organic carbon that drives the oxygen demand with the tidal flow. The oxygen concentration temporarily dropped to hypoxic levels in summer on a daily scale. High transport of organic matter from the tidal marshes enhanced heterotrophic respiration in the estuary. In addition, tidal marshes tend to be modifiers of nutrients. Tidal marshes played an important role in the settling of particulate matter. The low-DO events in the tidal marshes and adjacent channels further increased the bottom phosphate release and denitrification, which enhanced phosphorus releases from the sediment but increased the removal of nitrogen from the system. In addition, estuarine phytoplankton production and other biochemical processes were also impacted by the tidal marshes, but phytoplankton production is mainly limited by transport processes and light. Overall, the upstream marshes were found to exert a substantial influence on biochemical processes in the estuary. This developed model tends to advance the studies of marsh biogeochemistry by incorporating both the estuarine and wetland processes into a fully-looped system.

## Data Availability Statement

Data and metadata are available in the Github repository at [https://github.com/nicolecx122/ModelRole\\_JGRBGC](https://github.com/nicolecx122/ModelRole_JGRBGC) (<https://doi.org/10.5281/zenodo.7352036>; <https://zenodo.org/badge/latest/doi/508047127>).

## Acknowledgments

This research was financially supported by the Virginia Commonwealth Research Fellowship and supported in part by an appointment to the Research Participation Program at the Chesapeake Bay Program Office, U.S. Environmental Protection Agency, Region 3, administered by the Oak Ridge Institute for Science and Education through an interagency agreement between the U.S. Department of Energy and the U.S. Environmental Protection Agency. The authors received tremendous guidance and supports from Drs. Carl Cerco, Carl Hershner, Mark Brush, and Marjy Friedrichs in this study. The authors thank Dr. James Perry for providing photos of the York River Marshes for reference and as covering images. Simulations presented in this paper were conducted using Scilone at William & Mary, which was provided with assistance from the National Science Foundation, the Virginia Port Authority, Virginia's Commonwealth Technology Research Fund, and the Office of Naval Research.

## References

- Alongi, D. M. (2020). *Coastal ecosystem processes*. CRC press. <https://doi.org/10.1201/9781003057864>
- Anderson, I. C., Tobias, C. R., Neikirk, B. B., & Wetzel, R. L. (1997). Development of a process-based nitrogen mass balance model for a Virginia (USA) Spartina alterniflora salt marsh: Implications for net DIN flux. *Marine Ecology Progress Series*, 159, 13–27. <https://doi.org/10.3354/meps159013>
- Axelrad, D. M., Moore, K. A., & Bender, M. E. (1976). Nitrogen phosphorus and carbon flux in Chesapeake Bay marshes. Retrieved from <https://scholarworks.wm.edu/reports/2025>
- Bowden, W. B. (1986). Nitrification, nitrate reduction, and nitrogen immobilization in a tidal freshwater marsh sediment. *Ecology*, 67(1), 88–99. <https://doi.org/10.2307/1938506>
- Bowden, W. B., Vörösmarty, C. J., Morris, J. T., Peterson, B. J., Hobbie, J. E., Stuedler, P. A., & Moore, B., III. (1991). Transport and processing of nitrogen in a tidal freshwater wetland. *Water Resources Research*, 27(3), 389–408. <https://doi.org/10.1029/90WR02614>
- Bridgman, S. D., Megonigal, J. P., Keller, J. K., Bliss, N. B., & Trettin, C. (2006). The carbon balance of North American wetlands. *Wetlands*, 26(4), 889–916. [https://doi.org/10.1672/0277-5212\(2006\)26\[79:TEOALU\]2.0.CO;2](https://doi.org/10.1672/0277-5212(2006)26[79:TEOALU]2.0.CO;2)
- Brooks, T. J. (1983). Pamunkey River slack water data report: Temperature, salinity, dissolved oxygen (pp. 1970–1980). <https://doi.org/10.21220/V5XC76>
- Bukaveckas, P. A. (2021). Changes in acidity, DOC, and water clarity of Adirondack lakes over a 30-year span. *Aquatic Sciences*, 83(3), 50. <https://doi.org/10.1007/s00027-021-00807-6>
- Buzzelli, C. P., Wetzel, R. L., & Meyers, M. B. (1999). A linked physical and biological framework to assess biogeochemical dynamics in a shallow estuarine ecosystem. *Estuarine, Coastal and Shelf Science*, 49(6), 829–851. <https://doi.org/10.1006/ecss.1999.0556>
- Cai, X. (2018). *Impact of submerged aquatic vegetation on water quality in cache slough complex, Sacramento-San Joaquin delta: A numerical modeling study*. The College of William and Mary. Retrieved from <https://proxy.wm.edu/login?url=https://www.proquest.com/dissertations-theses/impact-submerged-aquatic-vegetation-on-water/docview/2092730456/se-2?accountid=15053>
- Cai, X., Qin, Q., Shen, J., & Zhang, Y. J. (2022). Bifurcate responses of tidal range to sea-level rise in estuaries with marsh evolution. *Limnology and Oceanography Letters*, 7(3), 210–217. <https://doi.org/10.1002/lol2.10256>
- Cai, X., Shen, J., Zhang, Y. J., Qin, Q., & Liner, L. (2022). The roles of tidal marshes in the estuarine biochemical processes: A numerical modeling study. Dataset. *Zenodo*. <https://doi.org/10.5281/zenodo.7352036>
- Cai, X., Zhang, Y. J., Shen, J., Wang, H., Wang, Z., Qin, Q., & Ye, F. (2020). A numerical study of hypoxia in Chesapeake Bay using an unstructured grid model: Validation and sensitivity to bathymetry representation. *JAWRA Journal of the American Water Resources Association*, 58(6), 898–921. <https://doi.org/10.1111/1752-1688.12887>
- Cerco, C., & Noel, M. (2017). *The 2017 Chesapeake Bay water quality and sediment transport model*. US Army Engineer Waterways Experiment Station. Retrieved from [https://www.chesapeakebay.net/documents/2017\\_WQSTM\\_Documentation\\_DRAFT\\_5-10-17.pdf](https://www.chesapeakebay.net/documents/2017_WQSTM_Documentation_DRAFT_5-10-17.pdf)
- Cerco, C. F., & Cole, T. M. (1994). *Three-dimensional eutrophication model of Chesapeake Bay. Volume 1: Main report. Final report* (No. AD-A-280760/0/XAB; WES/TR/EL-94-4). Army Engineer Waterways Experiment Station, Environmental Lab.
- Cerco, C. F., & Moore, K. (2001). System-wide submerged aquatic vegetation model for Chesapeake Bay. *Estuaries*, 24(4), 522–534. <https://doi.org/10.2307/1353254>
- Cerco, C. F., & Seitzinger, S. P. (1997). Measured and modeled effects of benthic algae on eutrophication in Indian River-Rehoboth Bay, Delaware. *Estuaries*, 20(1), 231–248. <https://doi.org/10.2307/1352733>
- Cerco, C. F., & Tian, R. (2021). Impact of wetlands loss and migration, induced by climate change, on Chesapeake Bay DO standards. *JAWRA Journal of the American Water Resources Association*, 58(6), 958–970. <https://doi.org/10.1111/1752-1688.12919>
- Cerco, C. F., & Tian, R. (2022). Impact of wetlands loss and migration, induced by climate change, on Chesapeake Bay DO Standards. *JAWRA Journal of the American Water Resources Association*, 58(6), 958–970. <https://doi.org/10.1111/1752-1688.12919>
- Chambers, R. M., Harvey, J. W., & Odum, W. E. (1992). Ammonium and phosphate dynamics in a Virginia salt marsh. *Estuaries*, 15(3), 349–359. <https://doi.org/10.2307/1352782>
- Chen, X., Santos, I. R., Hu, D., Zhan, L., Zhang, Y., Zhao, Z., & Li, L. (2022). Pore-water exchange flushes blue carbon from intertidal saltmarsh sediments into the sea. *Limnology and Oceanography Letters*, 7(4), 312–320. <https://doi.org/10.1002/lol2.10236>
- Chícharo, A., Chícharo, L., & Wolanski, E. (2008). Estuarine ecohdrology. In *Ecological engineering: Encyclopedia of ecology* (pp. 1413–1422). Retrieved from <https://sapientia.ualg.pt/handle/10400.1/2500>
- Chmura, G. L., Anisfeld, S. C., Cahoon, D. R., & Lynch, J. C. (2003). Global carbon sequestration in tidal, saline wetland soils. *Global Biogeochemical Cycles*, 17(4). <https://doi.org/10.1029/2002GB001917>
- Czapla, K. M., Anderson, I. C., & Currin, C. A. (2020). Net ecosystem carbon balance in a North Carolina, USA, salt marsh. *Journal of Geophysical Research: Biogeosciences*, 125(10), e2019JG005509. <https://doi.org/10.1029/2019JG005509>
- Davies, S. B. (2004). Vegetation dynamics of a tidal freshwater marsh: Long-term and inter-annual variability and their relationship to salinity. <https://doi.org/10.25773/v5-3ghv-5c27>
- DeLaune, R. D., Reddy, C. N., & Patrick, W. H. (1981). Accumulation of plant nutrients and heavy metals through sedimentation processes and accretion in a Louisiana salt marsh. *Estuaries*, 4(4), 328–334. <https://doi.org/10.2307/1352157>
- Diaz, R. J., & Rosenberg, R. (2001). Overview of anthropogenically-induced hypoxic effects on marine benthic fauna. *Coastal hypoxia: consequences for living resources and ecosystems*, 58, 129–145. <https://doi.org/10.1029/CE058p0129>
- Di Toro, D. M., & Fitzpatrick, J. J. (1993). *Chesapeake Bay sediment flux model*. Final Report (No. AD-A-267189/9/XAB). Hydroqual Inc.
- Fagherazzi, S., Kirwan, M. L., Mudd, S. M., Guntenspergen, G. R., Temmerman, S., D'Alpaos, A., et al. (2012). Numerical models of salt marsh evolution: Ecological, geomorphic, and climatic factors. *Reviews of Geophysics*, 50(1). <https://doi.org/10.1029/2011RG000359>
- Fagherazzi, S., Marani, M., & Blum, L. K. (2004). *The ecogeomorphology of tidal marshes*. American Geophysical Union. <https://doi.org/10.1029/CE059>
- Feijtel, T. C., DeLaune, R. D., & Patrick, W. H., Jr. (1985). Carbon flow in coastal Louisiana. *Marine ecology progress series. Oldendorf*, 24(3), 255–260. <https://doi.org/10.1029/24m024p255>

- Friedrichs, C. T. (2009). York River physical oceanography and sediment transport. *Journal of Coastal Research*, 10057(10057), 17–22. <https://doi.org/10.2112/1551-5036-57.sp1.17>
- Grant, R. R., & Patrick, R. (1970). *Tinicum Marsh as a water purifier* (pp. 105–131). Two Studies of Tinicum Marsh, Delaware and Philadelphia Counties, Pa. The Conservation Foundation.
- Hatton, R. S., Patrick, W. H., Jr., & DeLaune, R. D. (1982). Sedimentation, nutrient accumulation, and early diagenesis in Louisiana Barataria Basin coastal marshes. In *Estuarine comparisons* (pp. 255–267). Academic Press. <https://doi.org/10.1016/B978-0-12-404070-0.50021-1>
- Janousek, C. N., & Mayo, C. (2013). Plant responses to increased inundation and salt exposure: Interactive effects on tidal marsh productivity. *Plant Ecology*, 214(7), 917–928. <https://doi.org/10.1007/s11258-013-0218-6>
- Jordan, T. E., Correll, D. L., & Whigham, D. F. (1983). Nutrient flux in the rhode river: Tidal exchange of nutrients by brackish marshes. *Estuarine, Coastal and Shelf Science*, 17(6), 651–667. [https://doi.org/10.1016/0272-7714\(83\)90032-X](https://doi.org/10.1016/0272-7714(83)90032-X)
- Kirwan, M. L., & Murray, A. B. (2007). A coupled geomorphic and ecological model of tidal marsh evolution. *Proceedings of the National Academy of Sciences*, 104(15), 6118–6122. <https://doi.org/10.1073/pnas.0700958104>
- Knobloch, A. L., Reay, W. G., & Canuel, E. A. (2021). Carbon pools differ in source and temporal patterns in a tidal marsh creek system of the York River, VA Estuary. *Estuaries and Coasts*, 44(7), 1848–1865. <https://doi.org/10.1007/s12237-020-00878-y>
- Koch, F., & Gobler, C. J. (2009). The effects of tidal export from salt marsh ditches on estuarine water quality and plankton communities. *Estuaries and Coasts*, 32(2), 261–275. <https://doi.org/10.1007/s12237-008-9123-y>
- Lai, D. Y. F., & Lam, K. C. (2008). Phosphorus retention and release by sediments in the eutrophic Mai Po Marshes, Hong Kong. *Marine Pollution Bulletin*, 57(6–12), 349–356. <https://doi.org/10.1016/j.marpolbul.2008.01.038>
- Levin, L. A., Ekau, W., Gooday, A. J., Jorissen, F., Middelburg, J. J., Naqvi, S. W. A., et al. (2009). Effects of natural and human-induced hypoxia on coastal benthos. *Biogeosciences*, 6(10), 2063–2098. <https://doi.org/10.5194/bg-6-2063-2009>
- Li, Y., Yuan, L., Cao, H. B., Tang, C. D., Wang, X. Y., Tian, B., et al. (2021). A dynamic biomass model of emergent aquatic vegetation under different water levels and salinity. *Ecological Modelling*, 440, 109398. <https://doi.org/10.1016/j.ecolmodel.2020.109398>
- Izard, K., Hagen, S. C., Morris, J. T., Bacopoulos, P., Bilskie, M. V., Weishampel, J. F., & Medeiros, S. C. (2016). A coupled, two-dimensional hydrodynamic-marsh model with biological feedback. *Ecological Modelling*, 327, 29–43. <https://doi.org/10.1016/j.ecolmodel.2016.01.013>
- Marani, M., D'Alpaos, A., Lanzoni, S., Carniello, L., & Rinaldo, A. (2007). Biologically-controlled multiple equilibria of tidal landforms and the fate of the Venice lagoon. *Geophysical Research Letters*, 34(11), L11402. <https://doi.org/10.1029/2007GL030178>
- McHugh, J. M., & Dighton, J. (2004). Influence of mycorrhizal inoculation, inundation period, salinity, and phosphorus availability on the growth of two salt marsh grasses, *Spartina alterniflora* Loos. and *Spartina cynosuroides* (L.) Roth., in nursery systems. *Restoration Ecology*, 12(4), 533–545. <https://doi.org/10.1111/j.1061-2971.2004.03109.x>
- Mesinger, F., DiMego, G., Kalnay, E., Mitchell, K., Shafran, P. C., Ebisuzaki, W., et al. (2006). North American regional reanalysis. *Bulletin of the American Meteorological Society*, 87(3), 343–360. <https://doi.org/10.1175/BAMS-87-3-343>
- Mitchell, M., Herman, J., Bilkovic, D. M., & Hershner, C. (2017). Marsh persistence under sea-level rise is controlled by multiple, geologically variable stressors. *Ecosystem Health and Sustainability*, 3(10), 1379888. <https://doi.org/10.1080/20964129.2017.1396009>
- Moore, K. A. (2009). Submerged aquatic vegetation of the York River. *Journal of Coastal Research*, 10057(10057), 50–58. <https://doi.org/10.2112/1551-5036-57.sp1.50>
- Morris, J. T., Sundareshwar, P. V., Nietch, C. T., Kjerfve, B., & Cahoon, D. R. (2002). Responses of coastal wetlands to rising sea level. *Ecology*, 83(10), 2869–2877. [https://doi.org/10.1890/0012-9658\(2002\)083\[2869:ROCWTR\]2.0.CO;2](https://doi.org/10.1890/0012-9658(2002)083[2869:ROCWTR]2.0.CO;2)
- Neubauer, S. C., & Anderson, I. C. (2003). Transport of dissolved inorganic carbon from a tidal freshwater marsh to the York River estuary. *Limnology & Oceanography*, 48(1), 299–307. <https://doi.org/10.4319/lo.2003.48.1.0299>
- Nidzieko, N. J., Needoba, J. A., Monismith, S. G., & Johnson, K. S. (2014). Fortnightly tidal modulations affect net community production in a mesotidal estuary. *Estuaries and Coasts*, 37(1), 91–110. <https://doi.org/10.1007/s12237-013-9765-2>
- Odum, W. E., Smith, T. J., III, Hoover, J. K., & McIvor, C. C. (1984). *The ecology of tidal freshwater marshes of the United States east coast: A community profile*. US Fish Wildl. Serv. FWS/OBS-83/17.
- Pawlowicz, R., Beardsley, B., & Lentz, S. (2002). Classical tidal harmonic analysis including error estimates in MATLAB using T\_TIDE. *Computers & Geosciences*, 28(8), 929–937. [https://doi.org/10.1016/S0098-3004\(02\)00013-4](https://doi.org/10.1016/S0098-3004(02)00013-4)
- Pearcy, R. W., & Ustin, S. L. (1984). Effects of salinity on growth and photosynthesis of three California tidal marsh species. *Oecologia*, 62(1), 68–73. <https://doi.org/10.1007/bf00377375>
- Perry, J. E., & Hershner, C. H. (1999). Temporal changes in the vegetation pattern in a tidal freshwater marsh. *Wetlands*, 19(1), 90–99. <https://doi.org/10.1007/BF03161737>
- Perry, J. E., III. (1991). Analysis of vegetation patterns in a tidal freshwater marsh. Doctoral dissertation, The College of William and Mary. Retrieved from <https://proxy.wm.edu/login?url=https://www.proquest.com/dissertations-theses/analysis-vegetation-patterns-tidal-freshwater/docview/303922217/se-2?accountid=15053>
- Qin, Q., & Shen, J. (2019). Pelagic contribution to gross primary production dynamics in shallow areas of York River, VA, USA. *Limnology & Oceanography*, 64(4), 1484–1499. <https://doi.org/10.1002/lno.11129>
- Ridd, P., Sandstrom, M. W., & Wolanski, E. (1988). Outwelling from tropical tidal salt flats. *Estuarine, Coastal and Shelf Science*, 26(3), 243–253. [https://doi.org/10.1016/0272-7714\(88\)90063-7](https://doi.org/10.1016/0272-7714(88)90063-7)
- Roberts, D., MacVean, L., Holleman, R., Chelsky, A., Art, K., Nidzieko, N., et al. (2022). Connections to tidal marsh and restored salt ponds drive seasonal and spatial variability in ecosystem metabolic rates in Lower South San Francisco Bay. *Estuaries and Coasts*, 45(8), 2560–2577. <https://doi.org/10.1007/s12237-022-01088-4>
- Shen, J., & Haas, L. (2004). Calculating age and residence time in the tidal York River using three-dimensional model experiments. *Estuarine, Coastal and Shelf Science*, 61(3), 449–461. <https://doi.org/10.1016/j.ecss.2004.06.010>
- Shenk, G. W., & Linker, L. C. (2013). Development and application of the 2010 Chesapeake Bay watershed total maximum daily load model. *JAWRA Journal of the American Water Resources Association*, 49(5), 1042–1056. <https://doi.org/10.1111/jawr.12109>
- Sin, Y., Wetzel, R. L., & Anderson, I. C. (1999). Spatial and temporal characteristics of nutrient and phytoplankton dynamics in the York River estuary, Virginia: Analyses of long-term data. *Estuaries*, 22(2), 260–275. <https://doi.org/10.2307/1352982>
- Sundareshwar, P. V., Morris, J. T., Koepfler, E. K., & Fornwalt, B. (2003). Phosphorus limitation of coastal ecosystem processes. *Science*, 299(5606), 563–565. <https://doi.org/10.1126/science.1079100>
- Swarth, C., & Peters, D. (1993). *Water quality & nutrient dynamics of Jug Bay on the Patuxent river, 1987-1992*. Anne Arundel County, Department of Recreation and Parks, Jug Bay Wetlands Sanctuary.
- Townend, I., Fletcher, C., Knappen, M., & Rossington, K. (2011). A review of salt marsh dynamics. *Water and Environment Journal*, 25(4), 477–488. <https://doi.org/10.1111/j.1747-6593.2010.00243.x>

- Tzortziou, M., Neale, P. J., Megonigal, J. P., Pow, C. L., & Butterworth, M. (2011). Spatial gradients in dissolved carbon due to tidal marsh outwelling into a Chesapeake Bay estuary. *Marine Ecology Progress Series*, 426, 41–56. <https://doi.org/10.3354/meps09017>
- Watson, E. B., Andrews, H. M., Fischer, A., Cencer, M., Coiro, L., Kelley, S., & Wigand, C. (2015). Growth and photosynthesis responses of two co-occurring marsh grasses to inundation and varied nutrients. *Botany*, 93(10), 671–683. <https://doi.org/10.1139/cjb-2015-0055>
- Zhang, Y. J., Gerdtz, N., Ateljevich, E., & Nam, K. (2020). Simulating vegetation effects on flows in 3D using an unstructured grid model: Model development and validation. *Ocean Dynamics*, 70(2), 213–230. <https://doi.org/10.1007/s10236-019-01333-8>
- Zhang, Y. J., Ye, F., Stanev, E. V., & Grashorn, S. (2016). Seamless cross-scale modeling with SCHISM. *Ocean Modelling*, 102, 64–81. <https://doi.org/10.1016/j.ocemod.2016.05.002>
- Ziegler, S., Velinsky, D. J., Swarth, C. W., & Fogel, M. L. (1999). *Sediment-water exchange of dissolved inorganic nitrogen in a freshwater tidal wetland*. Technical report of the Jug Bay Wetlands Sanctuary. Anne Arundel County Parks.